

# ULRR

## **A mixed inverse differential quadrature method for static analysis of constant- and variable-stiffness laminated beams based on Hellinger-Reissner mixed variational formulation**

Item Type	Article
Authors	Trinh, Luan C.;Ojo, Saheed O.;Groh, Rainer M.J.;Weaver, Paul M.
Citation	International Journal of Solids and Structures;210–211, pp. 66-87
Publisher	Elsevier
Download date	2026-05-14 10:43:25
Item License	<a href="https://creativecommons.org/licenses/by-nc-sa/1.0/">https://creativecommons.org/licenses/by-nc-sa/1.0/</a>
Link to Item	<a href="https://hdl.handle.net/10344/9675">https://hdl.handle.net/10344/9675</a>



Contents lists available at ScienceDirect

## International Journal of Solids and Structures

journal homepage: [www.elsevier.com/locate/ijsostr](http://www.elsevier.com/locate/ijsostr)

# A mixed inverse differential quadrature method for static analysis of constant- and variable-stiffness laminated beams based on Hellinger-Reissner mixed variational formulation

Luan C. Trinh<sup>a,\*</sup>, Saheed O. Ojo<sup>a</sup>, Rainer M.J. Groh<sup>b</sup>, Paul M. Weaver<sup>a,b</sup><sup>a</sup> Bernal Institute, School of Engineering, University of Limerick, Castletroy V94 T9PX, Ireland<sup>b</sup> Bristol Composites Institute (ACCIS), Department of Aerospace Engineering, University of Bristol, Queen's Building, University Walk, Bristol BS8 1TR, UK

## ARTICLE INFO

## Article history:

Received 21 April 2020

Received in revised form 28 October 2020

Accepted 16 November 2020

Available online 23 November 2020

## Keywords:

Inverse differential quadrature method

Hellinger-Reissner mixed formulation

Variable stiffness beam

Zigzag theory

Stress analysis

Interlaminar condition

## ABSTRACT

Increasing applications of laminated composite structures necessitate the development of equivalent single layer (ESL) models that can achieve similar accuracy but are more computationally efficient than 3D or layer-wise models. Most ESL displacement-based models do not guarantee interfacial continuity of shear stresses within laminates. A possible remedy is the enforcement of interlaminar equilibrium in variational formulations, for example, in the framework of the Hellinger-Reissner variational principle, leading to a mixed force/displacement model. In this paper, the governing equations for bending and stretching of laminated beams, comprising only seven stress resultants and two displacement functionals, are obtained using global fifth-order and a local linear zigzag kinematics. As a strong-form solution technique, the differential quadrature method (DQM) is an efficient tool which can provide excellent convergence with relatively few number of grid points. However, in dealing with high-order differential equations, the conventional DQM can incur considerable errors due to the nature of numerical differentiation. Therefore, a mixed inverse differential quadrature method (iDQM) is proposed herein to solve the governing fourth-order differential equations for bending and stretching of laminated beams. This approach involves approximating the first derivatives of functional unknowns, thereby reducing the order of differentiation being performed. Using a non-uniform Chebychev-Gauss-Lobatto grid point profile, numerical results show that the accuracy of stress predictions is improved by using iDQM compared to DQM. In addition, the Cauchy's equilibrium condition is satisfied more accurately by iDQM, especially in the vicinity of boundaries.

© 2020 The Authors. Published by Elsevier Ltd. This is an open access article under the CC BY license (<http://creativecommons.org/licenses/by/4.0/>).

## 1. Introduction

The design of multi-layered composite structures requires accurate prediction of stress to guarantee safe design of primary load-bearing components. In many seemingly one-dimensional structures, the cross-sectional dimensions can approach the order of the span-wise dimension, such as the wall thickness of wind turbine blades and aircraft wings. In these structures, the effects of shear stress and transverse normal stress are important for both global and localised behaviours.

Euler-Bernoulli-based models, which were formulated from classical beam theory (CBT) (Jones, 1998), are inadequate for capturing through-thickness stress fields for thick structures. In order to improve the accuracy yet maintain the computational efficiency

of Euler-Bernoulli-based models, different displacement-based models have been proposed to model cross-sectional distortion and account for the effects of transverse stresses. Examples of these non-classical models include the first-order shear deformation beam theory (Timoshenko and Goodier, 1970) which accounts for a uniform shear strain through thickness, and Levinson-Reddy-type higher-order shear deformation theories (HSDT) (Ferreira et al., 2014; Mantari and Canales, 2016; Mantari et al., 2012; Vo et al., 2017; Vo and Thai, 2012; Zenkour, 1999), which satisfy the condition of vanishing shear stress on the outer surfaces. One of the drawbacks of HSDTs is that the axial displacement is at least  $C_z^1$ -continuous through-the-thickness, such that the interfacial continuity condition of shear stresses among laminae of different shear rigidity cannot be fulfilled from the constitutive relation.

To this effect, zigzag theories were proposed by (Lekhnitskii, 1935; Ambartsumian, 1958; Di Sciuva, 1984), and (Tessler et al., 2007, 2009). Zigzag theories are advanced equivalent single layer

\* Corresponding author.

E-mail address: [luan.trinh@ul.ie](mailto:luan.trinh@ul.ie) (L.C. Trinh).

models which can integrate changes in layer-wise slopes of the in-plane displacements in the kinematic assumption. Among them, the refined zigzag theory (RZT) by Tessler and co-authors performs well in analysing various sandwich and laminated structures. However, for thick laminates or for the stress calculation near the boundaries, higher-order displacements are needed to improve accuracy. In combination with a higher-order global displacement field (Groh and Weaver, 2015), the results from models based on zigzag kinematics match well with those from Pagano's exact solutions or 3D finite element analysis for generally laminated beams except for discrepancies observed in the immediate vicinity of boundaries. Successful applications of RZT to different analyses of beams and plates can be found in many recent publications (Barut et al., 2012, 2013; Di Sciuva and Sorrenti, 2019; Fares and Elmarghany, 2008; Flores et al., 2018; Groh et al., 2015; Groh, 2015; Iurlaro et al., 2015a, 2015b; Nallim et al., 2017; Tessler, 2015; Versino et al., 2014). For displacement-based theories, all stresses are derived from axiomatic displacement fields and their derivatives. As a result, the transverse stresses typically do not satisfy the interfacial continuity requirements and a post-processing step based on Cauchy's indefinite equilibrium conditions is required (Groh and Tessler, 2017). Because these post-processed stresses are different from those computed from a constitutive law, they are variationally inconsistent. In mixed variational statements, such as the Hellinger-Reissner principle, the equilibrium conditions can be included in the variational formulation by using Lagrange multipliers. This procedure ensures equilibrated stress fields and accurate stress predictions (Batra and Vidoli, 2002; Groh and Weaver, 2016; Tessler, 2015). Some important contributions to this interesting mixed variational principle can be mentioned for one-dimensional (Auricchio et al., 2010, 2015; Özütok and Madenci, 2017), two-dimensional (Auricchio et al., 2014; Madeo et al., 2014; Nguyen and Ibrahimbegovic, 2020; Zucco et al., 2016) and three-dimensional problems (Faghih Shojaei and Yavari, 2019; Viebahn et al., 2018).

Many problems in engineering and science involve finding solutions to differential equations. The finite element method (Hughes, 1987; Reddy, 2006) and the finite difference method (Smith, 1985) are among the most popular discretization techniques used in solving these equations. For example, the finite element method discretises the domain into subdomains (elements) and functionals and their derivatives are approximated over these elements. The accuracy of solutions mainly depends on the mesh density. As an alternative, higher-order methods have become more popular in recent years. Some well-known higher-order approaches include radial basis function networks (Ferreira et al., 2011; Mai-Duy and Tran-Cong, 2001, 2003), element free Galerkin methods (Hegen, 1996; Lu et al., 1994), isogeometric analysis (Cottrell et al., 2009), hierarchical finite element methods (Taylor et al., 1998), differential quadrature method (DQM) (Bacciocchi et al., 2016; Bellman et al., 1972; Bert and Malik, 1996; Ferreira et al., 2014; Liew et al., 2003; Ojo et al., 2019; Shu, 2000; Tornabene et al., 2014; Zong and Zhang, 2009) and combinations of different approaches (Eftekhari et al., 2009; Eftekhari and Jafari, 2012; Fantuzzi et al., 2015, 2014; Liu et al., 2017; Mittal and Rohila, 2016; Wu et al., 2018). The common feature of these higher-order methods is that the approximation function can be constructed over adjacent points (local support) or over the entire domain (global support). In most of higher-order methods, the functional derivatives are approximated numerically from weighting coefficients derived from derivatives of interpolation functions. This procedure may amplify numerical error, especially cumulative error in higher-order derivatives, due to the sensitivity of numerical differentiation to inherent function approximation error, as discussed in (Mai-Duy and Tran-Cong, 2003; Ngo-Cong et al., 2010, 2011; Wu and Ren, 2007). According to these papers, numerical integration

is more stable and less prone to numerical error suggesting an 'indirect' approximation of higher-order variables in a system and recovery of the original variable via integration. This approach led to the development of "indirect radial basis function networks" in (Mai-Duy and Tran-Cong, 2003) and the differential quadrature method based on approximation of the highest derivatives (DQIHD) in (Wu and Ren, 2007). To further generalise the application of the DQIHD method, (Ojo et al., 2020) proposed a novel inverse differential quadrature method (iDQM) by developing an efficient routine which relies on the inversion of the existing DQM formula to obtain accurate solutions of high-order differential equations. Potentially, according to mathematical analysis in (Ojo et al., 2020), the iDQM is robust, accurate and possesses superior numerical stability compared to DQM due to its ability to combine the advantages of numerical integration and numerical differentiation for system solution. It is worth mentioning that 'indirect' approximation leads to the introduction of integration constants in the system equations, resulting in a non-square global matrix.

In this study, we explore the prospects of the newly developed iDQM for numerical analysis of mechanical systems. Specifically, the paper proposes a mixed iDQM to obtain the solution of the Hellinger-Reissner mixed variational formulation based on fifth-order global and linear zigzag kinematics for static analysis of both constant- and variable-stiffness laminated beams. In the mixed iDQM framework, a combination of DQM and iDQM strategies is adopted to approximate an intermediate high-order variable in the system of equations and subsequently obtain higher-order variable or lower-order variables by DQM or iDQM operations, respectively. Through this approach, we are able to accomplish a reduction of differentiation order of the system equations and incorporate the computational advantages of numerical integration in the solution process.

The rest of paper is organised as follows. Section 2 presents the derivation of governing and boundary equations obtained from a higher-order zigzag displacement theory within the framework of the Hellinger-Reissner mixed variational principle. Subsequently, formulations of the differential quadrature method and the mixed inverse differential quadrature method are presented. In Section 3, flexural analysis of constant- and variable-stiffness laminated beams under different boundary conditions is conducted. The accuracy of stress predictions near clamped and free boundaries is studied in detail. Finally, conclusions are drawn in Section 4.

## 2. Mathematical formulation

### 2.1. Higher-order zigzag displacement theory

Consider a laminated beam of length  $L$ , rectangular cross-section of width  $b$  and thickness  $t$ . The beam comprises  $N$  layers which can be of arbitrary material properties such as constant orthotropic (e.g. straight-fibre reinforced plastic), varying orthotropic (e.g. variable angle tow (VAT) composite), or isotropic materials. The beam is referenced in a Cartesian coordinate system  $(x, y, z)$  with  $x \in [0, L]$  defining the longitudinal dimension,  $y \in [0, b]$  the width and  $z \in [-t/2, t/2]$  being the thickness direction as depicted in Fig. 1. By employing higher-order through-thickness kinematics, the structure is converted to a 1D problem, i.e. equivalent single layer (ESL) model, aligned along the  $x$ -direction where the geometry/material properties at each axial location represent integrated properties over the cross-section  $b \times t$ . The third-order refined zigzag in-plane displacement field initially proposed by (Groh and Weaver, 2015) is here enhanced to a fifth-order zigzag theory. Therefore, the longitudinal and transverse displacements are assumed as follows

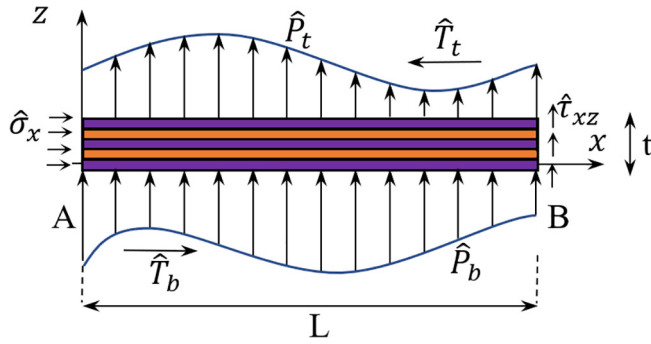


**Fig. 1.** Configuration of laminated beam with external tractions at top, bottom surfaces and beam ends A and B.

$$u_x^{(k)}(x, z) = u_0 + zu_1 + z^2u_2 + z^3u_3 + z^4u_4 + z^5u_5 + \phi^{(k)}(x, z)u_{zz} \quad (1a)$$

$$u_z(x) = w_0 \quad (1b)$$

where  $\mathbf{f}_{\phi_u}^{(k)}(x, z) = [1 \ z \ z^2 \ z^3 \ z^4 \ z^5 \ \phi^{(k)}(x, z)]$  is a shape function matrix defining the thickness-wise displacement's configuration and  $u = [u_0 \ u_1 \ u_2 \ u_3 \ u_4 \ u_5 \ u_{zz}]^T$  is the corresponding displacement vector. The first six components of  $u$  are global expansion terms through thickness while the last term  $u_{zz}$  is associated with a linear zigzag function of the form  $\phi^{(k)}(x, z) = m^{(k)}(x)z + c^{(k)}(x)$ . This zigzag term imposes a local displacement field on each ply  $k$ . In this paper, two zigzag models are considered. The first model was proposed by (Tessler et al., 2007), known as the Refined Zigzag Theory (RZT), in which the linear zigzag function is defined from the transverse shear modulus and thicknesses of each lamina in the laminate. This zigzag function is determined for all layers in a recursive form to superimpose the local displacement onto each ply. For the first and  $k^{\text{th}}$  layers the RZT zigzag function (Groh and Weaver, 2015; Tessler et al., 2007) reads

$$\phi_{RZT}^{(1)}(x, z) = \left[ \frac{G(x)}{G_{xz}^{(1)}(x, z)} - 1 \right] \left( z + \frac{t}{2} \right), \quad (2a)$$

$$\begin{aligned} \phi_{RZT}^{(k)}(x, z) = & \left[ \frac{G(x)}{G_{xz}^{(k)}(x, z)} - 1 \right] \left( z + \frac{t}{2} \right) \\ & + \sum_{j=2}^k t^{(j-1)} \left[ \frac{G(x)}{G_{xz}^{(j-1)}(x, z)} - \frac{G(x)}{G_{xz}^{(k)}(x, z)} \right], \text{ for } k = 2, \dots, N \end{aligned} \quad (2b)$$

where  $G_{xz}^{(k)}(x, z)$  is the transverse shear modulus of the  $k^{\text{th}}$  layer and  $G(x) = \left[ \frac{1}{t} \sum_{k=1}^N \frac{t^{(k)}}{G_{xz}^{(k)}} \right]^{-1}$  is the equivalent shear modulus of the laminate. The second zigzag function to be implemented was proposed by (Murakami, 1986) and is defined based on the ply thickness only, i.e.

$$\phi_{MZZF}^{(k)}(z) = (-1)^k \frac{2}{t^{(k)}} (z - z_m^{(k)}) \quad (3)$$

where  $t^{(k)}$  and  $z_m^{(k)}$  are the thickness and midplane coordinate of the  $k^{\text{th}}$  layer.

As discussed in chapter 6 of Groh (Groh, 2015; Groh et al., 2015), implementing RZT in variable angle tow laminates can lead to numerical instabilities if a discretisation point happens to have a constant  $G_{xz}^{(k)}(x, z)$  through the thickness or no uniquely definable spanwise derivative of  $G_{xz}^{(k)}(x, z)$ . Therefore, RZT is used for constant stiffness beams while MZZF is used for VAT laminated beams in this paper. This simplifies the zigzag functions to  $z$ -dependent

only, hence, the linear in-plane strain can be derived from the kinematics in Eq. (1),

$$\varepsilon_x^{(k)} = \frac{\partial u_x}{\partial x} = \mathbf{f}_{\phi_u}^{(k)} U_x = \mathbf{f}_{\phi_u}^{(k)} \boldsymbol{\varepsilon} \quad (4)$$

where  $\boldsymbol{\varepsilon} = U_x$  is an equivalent strain vector of the beam's midplane, and the comma notation represents differentiation. Neglecting the effect of transverse normal strain  $\varepsilon_z^{(k)}$ , the axial stress is expressed through the strain vector as

$$\sigma_x^{(k)} = \bar{Q}_{xx}^{-(k)} \varepsilon_x^{(k)} = \bar{Q}_{xx}^{-(k)} \mathbf{f}_{\phi_u}^{(k)} \boldsymbol{\varepsilon} \quad (5)$$

where  $\bar{Q}_{xx}^{-(k)}$  is the transformed in-plane material stiffness of layer  $k$ . The stress resultants are then derived by integrating the product of stress  $\sigma_x^{(k)}$  (from Eq. (5)) and the assumed strain shape function  $\mathbf{f}_{\phi_u}^{(k)}$  (from Eq. (4)) as follows

$$\mathcal{F} = \int_{-t/2}^{t/2} \sigma_x^{(k)} \mathbf{f}_{\phi_u}^{(k)T} dz = \int_{-t/2}^{t/2} \mathbf{f}_{\phi_u}^{(k)T} \bar{Q}_{xx}^{-(k)} \mathbf{f}_{\phi_u}^{(k)} dz \boldsymbol{\varepsilon} = \mathbf{S} \boldsymbol{\varepsilon} \quad (6)$$

where the higher-order ABD matrix  $\mathbf{S}$  is defined as

$$\mathbf{S} = \begin{bmatrix} A & B & D & E & F & H & B_\phi \\ B & D & E & F & H & I & D_\phi \\ D & E & F & H & I & J & E_\phi \\ E & F & H & I & J & R & F_\phi \\ F & H & I & J & R & S & H_\phi \\ H & I & J & R & S & T & I_\phi \\ B_\phi & D_\phi & E_\phi & F_\phi & H_\phi & I_\phi & D_{\phi\phi} \end{bmatrix} \quad (7)$$

and the beam stiffness constants are evaluated by the following integrals,

$$(A, B, D) = \sum_{k=1}^N \int_{z_k}^{z_{k+1}} \bar{Q}_{xx}^{-(k)} (1, z, z^2) dz \quad (8a)$$

$$(E, F, H, I, J, R, S, T) = \sum_{k=1}^N \int_{z_k}^{z_{k+1}} \bar{Q}_{xx}^{-(k)} (z^3, z^4, z^5, z^6, z^7, z^8, z^9, z^{10}) dz \quad (8b)$$

$$(B_\phi, D_\phi) = \sum_{k=1}^N \int_{z_k}^{z_{k+1}} \bar{Q}_{xx}^{-(k)} \phi^{(k)}(1, z) dz \quad (8c)$$

$$(E_\phi, F_\phi, H_\phi, I_\phi, D_{\phi\phi}) = \sum_{k=1}^N \int_{z_k}^{z_{k+1}} \bar{Q}_{xx}^{-(k)} \phi^{(k)}(z^2, z^3, z^4, z^5, \phi^{(k)}) dz \quad (8d)$$

where  $z_{k-1}$  and  $z_k$  indicate the lower and upper coordinate of the  $k^{\text{th}}$  lamina.

To obtain the governing and boundary equations, a conventional approach expresses all stress resultants in terms of the displacement variables using Eq. (6), and then implements a variational principle to minimise strain energy with respect to the displacement functionals, i.e. displacement-based solutions. However, alternative approaches can be used to derive differential equations associated with stress resultants (Groh and Weaver, 2015, 2016; Thurnherr et al., 2016) or generalised strains (Trinh et al., 2020) in which lower-order differential equations are obtained. Here, a well-developed approach based on the Hellinger-Reissner mixed variational principle (Groh and Weaver, 2015) is employed. According to the Hellinger-Reissner principle, stresses and displacements are treated as independent fields in seeking a minimum total potential energy state of the deformed structure. In the more contracted form of a 1D beam problem, stress resultants and corresponding displacements are functional

unknowns in the variational principle. To obtain an expression for the strains in terms of the stress resultants, we simply invert Eq. (6) to get

$$\boldsymbol{\varepsilon} = \mathbf{s}\mathcal{F} \quad (9)$$

where  $\mathbf{s}$  is the inversion of  $\mathbf{S}$ . Using this expression, the in-plane stress can be expressed in terms of the one-dimensional stress resultant functionals  $\mathcal{F}$  as

$$\boldsymbol{\sigma}_x^{(k)} = \bar{Q}_{xx}^{(k)} \mathbf{f}_{\phi_u}^{(k)} \boldsymbol{\varepsilon} = \bar{Q}_{xx}^{(k)} \mathbf{f}_{\phi_u}^{(k)} \mathbf{s}\mathcal{F} \quad (10)$$

## 2.2. Derivation of shear stress and transverse normal stress

In this section, the expression for the transverse shear stress and the transverse normal stress are derived from the in-plane stress of Eq. (10) using Cauchy's indefinite equilibrium equations. In addition, the continuity of these stress components is guaranteed *a priori*. Firstly, the transverse shear stress is obtained by integrating in-plane stress in Eq. (10) through thickness

$$\tau_{xz}^{(k)} = - \int \sigma_{xx}^{(k)} dz = - \bar{Q}_{xx}^{(k)} \mathbf{g}_{\phi}^{(k)} \mathbf{s}\mathcal{F}_{,x} + \mathbf{a}^{(k)} \quad (11)$$

where  $\mathbf{g}_{\phi}^{(k)}$  is the through-thickness shape function of the transverse shear stress and is derived by z-wise integrating the axial shape function  $\mathbf{f}_{\phi_u}^{(k)}$ . The through-thickness constant vector  $\mathbf{a}^{(k)}$  can be expressed in terms of stress resultant functionals  $\mathcal{F}$  by enforcing interlaminar continuity conditions. This procedure is discussed in detail by (Groh and Weaver, 2015) and summarised below

$$\mathbf{a}^{(k)} = \boldsymbol{\alpha}^{(k)} \mathbf{s}\mathcal{F}_{,x} + \hat{\mathbf{T}}_b, \quad (12)$$

where

$$\boldsymbol{\alpha}^{(k)} = \sum_{i=1}^k \left[ \bar{Q}_{xx}^{(i)} \mathbf{g}_{\phi}^{(i)}(z_{i-1}) - \bar{Q}_{xx}^{(i-1)} \mathbf{g}_{\phi}^{(i-1)}(z_{i-1}) \right]. \quad (13)$$

Hence, the shear stress is expressed in terms of the stress resultants as follows

$$\tau_{xz}^{(k)} = \mathbf{c}^{(k)} \mathbf{s}\mathcal{F}_{,x} + \hat{\mathbf{T}}_b, \quad (14)$$

where

$$\mathbf{c}^{(k)} = - \bar{Q}_{xx}^{(k)} \mathbf{g}_{\phi}^{(k)} + \boldsymbol{\alpha}^{(k)} \quad (15)$$

Similarly, the normal transverse stress is calculated from the equilibrium equation as follows

$$\sigma_z^{(k)} = - \int \tau_{xz,x}^{(k)} dz = \left( \bar{Q}_{xx}^{(k)} \mathbf{h}_{\phi}^{(k)} - \boldsymbol{\alpha}^{(k)} z \right) \mathbf{s}\mathcal{F}_{xx} - \hat{\mathbf{T}}_{b,x} z + \mathbf{b}^{(k)}, \quad (16)$$

where

$$\mathbf{h}_{\phi}^{(k)} = \int \mathbf{g}_{\phi}^{(k)} dz. \quad (17a)$$

$$\mathbf{b}^{(k)} = \boldsymbol{\beta}^{(k)} \mathbf{s}\mathcal{F}_{,xx} + \hat{\mathbf{T}}_{b,x} z_0 + \hat{\mathbf{P}}_b, \quad (17b)$$

$$\begin{aligned} \boldsymbol{\beta}^{(k)} = & - \sum_{i=1}^k \left[ \bar{Q}_{xx}^{(i)} \mathbf{h}_{\phi}^{(i)}(z_{i-1}) - \bar{Q}_{xx}^{(i-1)} \mathbf{h}_{\phi}^{(i-1)}(z_{i-1}) \right] \\ & + \sum_{i=1}^k (\boldsymbol{\alpha}^{(i)} - \boldsymbol{\alpha}^{(i-1)}) z_{i-1}, \end{aligned} \quad (17c)$$

In a compact form, the transverse normal stress in Eq. (16) is expressed by

$$\sigma_z^{(k)} = \mathbf{e}^{(k)} \mathbf{s}\mathcal{F}_{,xx} - \hat{\mathbf{T}}_{b,x} (z - z_0) + \hat{\mathbf{P}}_b \quad (18)$$

where

$$\mathbf{e}^{(k)} = \bar{Q}_{xx}^{(k)} \mathbf{h}_{\phi}^{(k)} - \boldsymbol{\alpha}^{(k)} z + \boldsymbol{\beta}^{(k)}. \quad (19)$$

It was previously proven in (Groh and Weaver, 2015) that as long as the equilibrium condition is satisfied, the traction conditions on the top and bottom surfaces are satisfied automatically together with the fulfilment of stress continuity at the layer interfaces. It is necessary to describe the equivalent single layer (ESL) equilibrium equations, which will be enforced using Lagrange multipliers in the variational formulation of the next section. To obtain the ESL equilibrium equations, the two Cauchy equilibrium equations are integrated through the thickness as in Eqs. (20) and (21)

$$\begin{aligned} \int_{z_0}^{z_N} \left( \sigma_{xx}^{(k)} + \tau_{xz,z}^{(k)} \right) dz &= 0 \\ \therefore N_{,x} + \tau_{xz}^{(N)}(z_N) - \tau_{xz}^{(1)}(z_0) &= 0 \text{ or } N_{,x} + \hat{\mathbf{T}}_t - \hat{\mathbf{T}}_b = 0 \end{aligned} \quad (20)$$

and

$$\begin{aligned} \int_{z_0}^{z_N} \left( \tau_{xz,x}^{(k)} + \sigma_z^{(k)} \right) dz &= 0 \\ \therefore Q_{,x} + \sigma_z^{(N)}(z_N) - \sigma_z^{(1)}(z_0) &= 0 \text{ or } Q_{,x} + \hat{\mathbf{P}}_t - \hat{\mathbf{P}}_b = 0 \end{aligned} \quad (21)$$

where  $\tau_{xz}^{(N)}(z_N) = \hat{\mathbf{T}}_t$ ,  $\tau_{xz}^{(1)}(z_0) = \hat{\mathbf{T}}_b$ ,  $\sigma_z^{(N)}(z_N) = \hat{\mathbf{P}}_t$  and  $\sigma_z^{(1)}(z_0) = \hat{\mathbf{P}}_b$  are the applied shear and normal stresses on the top and bottom surfaces, as depicted in Fig. 1. Eq. (21) is further simplified by expressing the shear force  $Q$  with respect to moment  $M$ , which is a component of the vector stress resultant  $\mathcal{F}$ . Moment equilibrium is obtained by multiply Eq. (20) by  $z$  and integrated through thickness

$$\begin{aligned} \int_{z_0}^{z_N} z \left( \sigma_{xx}^{(k)} + \tau_{xz,z}^{(k)} \right) dz &= \int_{z_0}^{z_N} z \sigma_{xx}^{(k)} dz + \left( z \tau_{xz}^{(k)} \right) \Big|_{z=z_0}^{z=z_N} - \int_{z_0}^{z_N} \tau_{xz,z}^{(k)} dz \\ &= 0. \end{aligned} \quad (22)$$

By noting that  $\int_{z_0}^{z_N} z \sigma_{xx}^{(k)} dz = M_{,x}$  and  $\int_{z_0}^{z_N} \tau_{xz,z}^{(k)} dz = Q$ , Eq. (20) is reduced to

$$\begin{aligned} M_{,x} + \left( z_N \hat{\mathbf{T}}_t - z_0 \hat{\mathbf{T}}_b \right) - Q &= 0 \\ \therefore Q &= M_{,x} + \left( z_N \hat{\mathbf{T}}_t - z_0 \hat{\mathbf{T}}_b \right) = 0 \end{aligned} \quad (23)$$

Therefore, the ESL equilibrium in Eq. (21) becomes

$$M_{,xx} + \left( z_N \hat{\mathbf{T}}_{t,x} - z_0 \hat{\mathbf{T}}_{b,x} \right) + \hat{\mathbf{P}}_t - \hat{\mathbf{P}}_b = 0 \quad (24)$$

## 2.3. Hellinger-Reissner based variational formulation for laminated beams

The transverse shear strain is defined by using the constitutive equation

$$\gamma_{xz}^{(k)} = \frac{\tau_{xz}^{(k)}}{G_{xz}^{(k)}} = \frac{1}{G_{xz}^{(k)}} \left( \mathbf{c}^{(k)} \mathbf{s}\mathcal{F}_{,x} + \hat{\mathbf{T}}_b \right). \quad (25)$$

Similarly, the transverse normal strain  $\varepsilon_z^{(k)}$  is derived from the plane strain state in the  $y$ -direction using the full compliance matrix

$$\begin{aligned} \varepsilon_z^{(k)} &= R_{xz}^{(k)} \sigma_x^{(k)} + R_{zz}^{(k)} \sigma_z^{(k)} \\ &= R_{xz}^{(k)} \bar{Q}_{xx}^{(k)} \mathbf{f}_{\phi_u}^{(k)} \mathbf{s}\mathcal{F} + R_{zz}^{(k)} \left[ \mathbf{e}^{(k)} \mathbf{s}\mathcal{F}_{,xx} - \hat{\mathbf{T}}_{b,x} (z - z_0) + \hat{\mathbf{P}}_b \right], \end{aligned} \quad (26)$$

where  $R_{ij} = S_{ij} - \frac{S_{iy} S_{jy}}{S_{yy}}$ , and  $S_{ij}$  is the full material compliance matrix.

Following the Lagrange multipliers approach given in (Groh and Weaver, 2015), the first variation of the potential energy functional including potentials of the Lagrange multipliers is set to zero to achieve equilibrium of the system, such that,

$$0 = \delta\Pi = \delta\Pi_{\sigma_x} + \delta\Pi_{\tau_{xz}} + \delta\Pi_{\sigma_z} + \delta\Pi_{\Gamma} + \delta\Pi_{\lambda}, \quad (27)$$

in which, the variations of strain energy of axial stress  $\Pi_{\sigma_x}$ , transverse shear stress  $\Pi_{\tau_{xz}}$ , transverse normal stress  $\Pi_{\sigma_z}$ , and the strain energy by boundary tractions  $\Pi_{\Gamma}$  are presented as follows

$$\begin{aligned} \delta\Pi_{\sigma_x} &= \frac{1}{2} \delta \int \sigma_{xx}^{(k)T} \varepsilon_{xx}^{(k)} dV \\ &= \frac{1}{2} \delta \int \mathcal{F}^T \mathbf{s}^T \int \left( \mathbf{f}_{\phi}^{(k)T} \bar{\mathbf{Q}}_{xx}^{(k)} \mathbf{f}_{\phi}^{(k)} \right) dz \mathbf{s} \mathcal{F} dx = \int \mathcal{F}^T \mathbf{s} \delta \mathcal{F} dx, \end{aligned} \quad (28)$$

$$\begin{aligned} \delta\Pi_{\tau_{xz}} &= \delta \frac{1}{2} \int \tau_{xz}^{(k)T} \gamma_{xz}^{(k)} dV = \delta \frac{1}{2} \int \left[ \mathbf{c}^{(k)} \mathbf{s} \mathcal{F}_{,x} + \hat{\mathbf{T}}_b \right]^T \frac{1}{G_{xz}^{(k)}} \left[ \mathbf{c}^{(k)} \mathbf{s} \mathcal{F}_{,x} + \hat{\mathbf{T}}_b \right] dV \\ &= \int \left( \mathcal{F}_{,x}^T \boldsymbol{\eta} + \hat{\mathbf{T}}_b \boldsymbol{\iota} \right) \delta \mathcal{F}_{,x} dx \end{aligned} \quad (29)$$

$$\text{where } \boldsymbol{\eta} = \int_{z_0}^{z_N} \mathbf{c}^{(k)T} \frac{1}{G_{xz}^{(k)}} \mathbf{c}^{(k)} dz, \quad \boldsymbol{\iota} = \int_{z_0}^{z_N} \frac{1}{G_{xz}^{(k)}} \mathbf{c}^{(k)} dz. \quad (30)$$

$$\begin{aligned} \delta\Pi_{\sigma_z} &= \delta \frac{1}{2} \int \sigma_z^{(k)T} \varepsilon_z^{(k)} dV \\ &= \delta \frac{1}{2} \int \left[ \mathbf{e}^{(k)} \mathbf{s} \mathcal{F}_{,xx} - \hat{\mathbf{T}}_{b,x} (z - z_0) + \hat{\mathbf{P}}_b \right]^T \\ &\quad \times \left\{ R_{xx}^{(k)} \bar{\mathbf{Q}}_{xx}^{(k)} \mathbf{f}_{\phi_u}^{(k)} \mathbf{s} \mathcal{F} + R_{zz}^{(k)} \left[ \mathbf{e}^{(k)} \mathbf{s} \mathcal{F}_{,xx} - \hat{\mathbf{T}}_{b,x} (z - z_0) + \hat{\mathbf{P}}_b \right] \right\} dV \\ &= \int \left[ \mathcal{F}_{,xx}^T \boldsymbol{\omega} + \mathcal{F}_{,xxxx}^T \boldsymbol{\rho} - \hat{\mathbf{T}}_{b,x} \frac{\boldsymbol{\omega}_t}{2} - \hat{\mathbf{T}}_{b,xxx}^T \boldsymbol{\rho}_t + \hat{\mathbf{P}}_b \frac{\boldsymbol{\omega}_p}{2} + \hat{\mathbf{P}}_{b,xx}^T \boldsymbol{\rho}_p \right] \delta \mathcal{F} dx \\ &\quad + \left[ \mathcal{F}_{,x}^T \frac{\boldsymbol{\omega}}{2} + \mathcal{F}_{,xx}^T \boldsymbol{\rho} - \hat{\mathbf{T}}_{b,x} \boldsymbol{\rho}_t + \hat{\mathbf{P}}_b \boldsymbol{\rho}_p \right] \delta \mathcal{F}_x \Big|_0^L \\ &\quad - \left[ \mathcal{F}_{,x}^T \frac{\boldsymbol{\omega}}{2} + \mathcal{F}_{,xxxx}^T \boldsymbol{\rho} - \hat{\mathbf{T}}_{b,xx} \boldsymbol{\rho}_t + \hat{\mathbf{P}}_{b,x} \boldsymbol{\rho}_p \right] \delta \mathcal{F} \Big|_0^L \end{aligned} \quad (31)$$

where

$$\boldsymbol{\rho} = \mathbf{s}^T \left( \int_{z_0}^{z_N} \mathbf{e}^{(k)T} R_{zz}^{(k)} \mathbf{e}^{(k)} dz \right) \mathbf{s}; \quad \boldsymbol{\omega} = \mathbf{s}^T \left( \int_{z_0}^{z_N} \mathbf{e}^{(k)T} R_{xx}^{(k)} \bar{\mathbf{Q}}_{xx}^{(k)} \mathbf{f}_{\phi}^{(k)} dz \right) \mathbf{s}; \quad (32a)$$

$$\boldsymbol{\rho}_t = \left( \int_{z_0}^{z_N} R_{zz}^{(k)} (z - z_0) \mathbf{e}^{(k)} dz \right) \mathbf{s}; \quad \boldsymbol{\rho}_p = \left( \int_{z_0}^{z_N} R_{zz}^{(k)} \mathbf{e}^{(k)} dz \right) \mathbf{s}; \quad (32b)$$

$$\boldsymbol{\omega}_t = \left( \int_{z_0}^{z_N} R_{xz}^{(k)} (z - z_0) \bar{\mathbf{Q}}_{xx}^{(k)} \mathbf{f}_{\phi}^{(k)} dz \right) \mathbf{s}; \quad \boldsymbol{\omega}_p = \left( \int_{z_0}^{z_N} R_{xz}^{(k)} \bar{\mathbf{Q}}_{xx}^{(k)} \mathbf{f}_{\phi}^{(k)} dz \right) \mathbf{s} \quad (32c)$$

$$\delta\Pi_{\Gamma} = -[\delta \mathcal{F} \cdot \hat{\boldsymbol{\iota}} + \delta \mathbf{Q} \cdot \hat{\mathbf{w}}_0] \Big|_0^L = -[\delta \mathcal{F} \cdot \hat{\boldsymbol{\iota}} + \delta \mathbf{M}_{,x} \cdot \hat{\mathbf{w}}_0] \Big|_0^L \quad (33)$$

The Lagrange multipliers are employed to enforce the equilibrium equations Eqs. (20) and (24) in the variational statement through  $\Pi_{\lambda}$ . Its variation with respects to axial force and moment as well as the Lagrange multipliers is presented as following

$$\begin{aligned} \delta\Pi_{\lambda} &= \int \left[ N_{,x} + \left( \hat{\mathbf{T}}_t - \hat{\mathbf{T}}_b \right) \right] \delta \lambda_1 dx - \int \lambda_{1,x} \delta N dx + \lambda_1 \delta N_x \Big|_0^L \\ &\quad + \int \left( M_{,xx} + z_N \hat{\mathbf{T}}_{t,x} - z_0 \hat{\mathbf{T}}_{b,x} + \hat{\mathbf{P}}_t - \hat{\mathbf{P}}_b \right) \delta \lambda_2 dx \\ &\quad + \int \lambda_{2,xx} \delta M - \lambda_{2,x} \delta M \Big|_0^L + \lambda_2 \delta M_{,x} \Big|_0^L \end{aligned} \quad (34)$$

Substituting Eqs. (28)–(34) into Eq. (27) and collecting the corresponding terms of  $\delta \lambda_1$ ,  $\delta \lambda_2$  and  $\delta \mathcal{F}$ , the governing equations are obtained

$$\delta \lambda_1 : N_{,x} + \hat{\mathbf{T}}_t - \hat{\mathbf{T}}_b = 0 \quad (35a)$$

$$\delta \lambda_2 : M_{,xx} + z_N \hat{\mathbf{T}}_{t,x} - z_0 \hat{\mathbf{T}}_{b,x} + \hat{\mathbf{P}}_t - \hat{\mathbf{P}}_b = 0 \quad (35b)$$

$$\begin{aligned} \delta \mathcal{F} : \mathbf{s}^T \mathcal{F} - \left( \boldsymbol{\eta} - \boldsymbol{\omega} \right)^T \mathcal{F}_{,xx} + \boldsymbol{\rho}^T \mathcal{F}_{,xxxx} + \frac{\boldsymbol{\omega}_p^T}{2} \hat{\mathbf{P}}_b + \boldsymbol{\rho}_p^T \hat{\mathbf{P}}_{b,xx} \\ - \left( \boldsymbol{\iota} + \frac{\boldsymbol{\omega}_t}{2} \right)^T \hat{\mathbf{T}}_{b,x} - \boldsymbol{\rho}_t^T \hat{\mathbf{T}}_{b,xxx} + \boldsymbol{\Lambda}_{eq} = 0 \end{aligned} \quad (35c)$$

where

$$\boldsymbol{\Lambda}_{eq} = [-\lambda_{1,x} \quad \lambda_{2,xx} \quad 0 \quad 0 \quad 0 \quad 0 \quad 0]^T \quad (36)$$

The pertinent boundary conditions are given by

$$\begin{aligned} \delta \mathcal{F} = 0 \text{ or } \left( \boldsymbol{\eta} - \frac{\boldsymbol{\omega}}{2} \right)^T \mathcal{F}_x - \boldsymbol{\rho}^T \mathcal{F}_{,xxx} - \boldsymbol{\iota}^T \hat{\mathbf{T}}_b + \boldsymbol{\rho}_t^T \hat{\mathbf{T}}_{b,xx} - \boldsymbol{\rho}_p^T \hat{\mathbf{P}}_{b,x} \\ + \boldsymbol{\Lambda}_{bc1} = \hat{\boldsymbol{\iota}} \end{aligned} \quad (37a)$$

$$\delta \mathcal{F}_{,x} = 0 \text{ or } \frac{\boldsymbol{\omega}^T}{2} \mathcal{F} + \boldsymbol{\rho}^T \mathcal{F}_{,xx} - \boldsymbol{\rho}_t^T \hat{\mathbf{T}}_{b,x} + \boldsymbol{\rho}_p^T \hat{\mathbf{P}}_b + \boldsymbol{\Lambda}_{bc2} = \mathcal{W} \quad (37b)$$

where

$$\boldsymbol{\Lambda}_{bc1} = [\lambda_1 \quad -\lambda_{2,x} \quad 0 \quad 0 \quad 0 \quad 0 \quad 0]^T, \quad (38a)$$

$$\boldsymbol{\Lambda}_{bc2} = [0 \quad \lambda_2 \quad 0 \quad 0 \quad 0 \quad 0 \quad 0]^T, \quad (38b)$$

$\hat{\boldsymbol{\iota}} = [\hat{\boldsymbol{\iota}}_0 \quad 0 \quad 0 \quad 0 \quad 0 \quad 0 \quad 0]^T$  and  $\mathcal{W} = [\hat{\mathbf{w}}_0 \quad 0 \quad 0 \quad 0 \quad 0 \quad 0 \quad 0]^T$  are applied axial and transverse displacements.

#### 2.4. Differential quadrature method (DQM) and inverse differential quadrature method (iDQM)

##### 2.4.1. Differential quadrature method

Differential quadrature is a numerical approach proposed by (Bellman et al., 1972), which approximates partial derivatives of a field functional with respect to a spatial variable. This procedure of single-variable derivatives at an arbitrary point is usually associated with the computation of a linear weighted sum of functional values at specific grid points. The first partial derivative of function  $f(x)$  at the  $i^{\text{th}}$  grid point is approximated as

$$\frac{\partial f(x_i)}{\partial x} = f^{(1)}(x_i) \approx a_{ij}^{(1)} f(x_j) \text{ for } i, j = 1, \bar{N}_p, \quad (39)$$

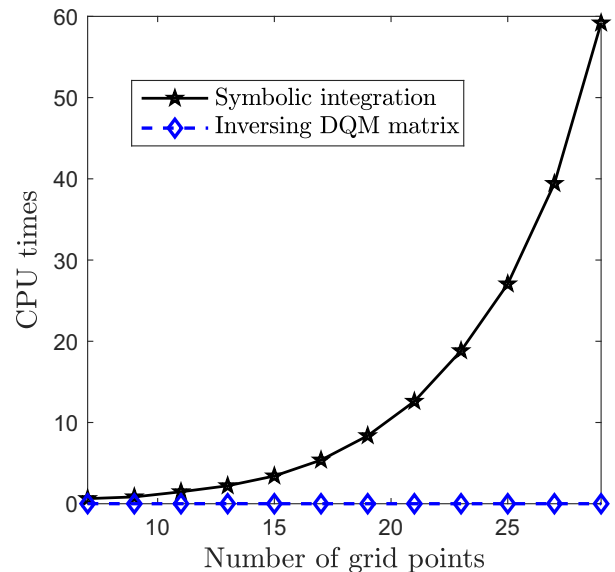


Fig. 2. Computing times by using symbolic integration in MATLAB and by inverting DQM matrix.

where  $x_j$  is the set of grid points in the x-direction,  $a_{ij}^{(1)}$  are the weighting coefficients of the first derivative, and Einstein summation rule is applied for repeated index  $j$  ranging from 1 to  $N_p$ , i.e.  $j = \overline{1, N_p}$ . A superscript in bracket  $(\cdot)$  indicates the order of derivatives. Analogously, the higher-order derivatives are expressed as

$$\frac{\partial f^n(x_i)}{\partial x^n} = f^{(n)}(x_i) \approx a_{ij}^{(n)} f(x_j) \text{ for } i, j = \overline{1, N_p}. \quad (40)$$

Following the generalised differential quadrature method by (Shu and Richards, 1992), in which the interpolating polynomials used in calculating the weighted coefficients are Lagrange polynomials, cardinal sine functions or Lagrange trigonometric polynomials, the interpolation coefficients are units at interpolated grid

points, i.e.  $i = j$ , and zeros at other grid points, i.e.  $i \neq j$ , hence the coefficient matrix is identity and always invertible. For example, the coefficient matrix  $l_k$  for a function approximation using the Lagrange polynomial basis (Quan and Chang, 1989) is determined by

$$l_k(x) = \frac{M(x)}{(x - x_k)M^{(1)}(x_k)} \text{ for } k = \overline{1, N_p}, \quad (41)$$

$$\text{where } M(x) = \prod_{i=1}^{N_p} (x - x_i) \text{ and } M^{(1)}(x_i) = \prod_{k=1, k \neq i}^{N_p} (x_i - x_k) \quad (42)$$

Substituting  $M(x)$  and  $M^{(1)}(x_i)$  into the coefficient matrix for the first derivative approximation  $l_k^{(1)}(x)$  at grid points  $x_j$  leads to

**Table 1**

Stacking sequence for constant stiffness laminates. The subscripts indicate the number of laminae repeating the pertinent property.

Laminate	Layer thickness ratio	Stacking sequence	Layer materials
<i>Simply-supported beams</i>			
SS <sub>1</sub>	[0.2 <sub>5</sub> ]	[90/0/90/0/90]	[p <sub>5</sub> ]
SS <sub>2</sub>	[(1/51) <sub>51</sub> ]	[0/(90/0) <sub>25</sub> ]	[p <sub>51</sub> ]
SS <sub>3</sub>	[0.1 <sub>2</sub> /0.2 <sub>3</sub> /0.1 <sub>2</sub> ]	[90/0 <sub>5</sub> /90]	[p <sub>2</sub> /pvc/h/pvc/p <sub>2</sub> ]
SS <sub>4</sub>	[0.1/0.3/0.35/0.25]	[0/90/0 <sub>2</sub> ]	[p <sub>2</sub> /m/p]
SS <sub>5</sub>	[0.3/0.2/0.15/0.25/0.1]	[0/90/0 <sub>2</sub> /90]	[p <sub>3</sub> /m/p]
<i>Cantilevered and clamped beams</i>			
CC <sub>1</sub> /CF	[(1/4) <sub>4</sub> ]	[0/90/0/90]	[p <sub>4</sub> ]
CC <sub>2</sub>	[(1/8) <sub>2</sub> /0.5/(1/8) <sub>2</sub> ]	[0/90/0 <sub>2</sub> /90]	[p <sub>2</sub> /pvc/p <sub>2</sub> ]
<i>Variable angle tow beams</i>			
VAT A	[(1/8) <sub>8</sub> ]	[(90/0)/(−90/0)/(45−45)/(−45/45)] <sub>8</sub>	[IM7 <sub>8</sub> ]
VAT B	[(1/8) <sub>8</sub> ]	[(90/20)/(45−25)/(−90−20)/(−45/25)] <sub>8</sub>	[IM7 <sub>8</sub> ]

**Table 2**

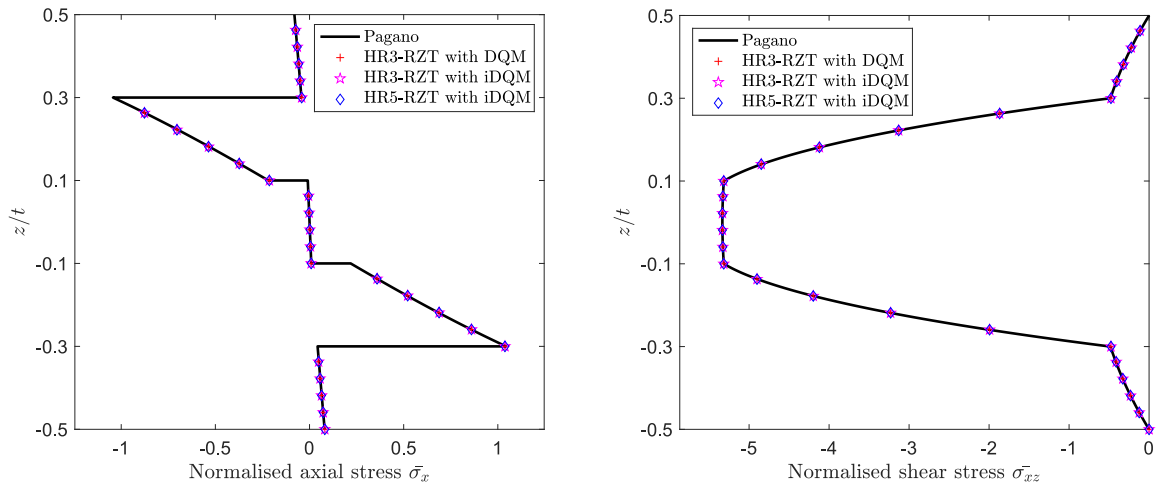
Mechanical properties of h, p, m, pvc and IM7 normalised by the in-plane modulus  $G_{12}^{(h)}$  of h.

Material	$\frac{E_1}{G_{12}^{(h)}}$	$\frac{E_2}{G_{12}^{(h)}}$	$\frac{E_3}{G_{12}^{(h)}}$	$\frac{G_{12}}{G_{12}^{(h)}}$	$\frac{G_{13}}{G_{12}^{(h)}}$	$\frac{G_{23}}{G_{12}^{(h)}}$	$\nu_{12}$	$\nu_{13}$	$\nu_{23}$
h	250.0	250.0	250.0	1.0	875.0	1750.0	0.9	$3.0 \times 10^{-5}$	$3.0 \times 10^{-5}$
p	$25.0 \times 10^6$	$1.0 \times 10^6$	$1.0 \times 10^6$	$5.0 \times 10^5$	$5.0 \times 10^5$	$2.0 \times 10^5$	0.25	0.25	0.25
m	$32.57 \times 10^6$	$1.0 \times 10^6$	$10.0 \times 10^6$	$6.5 \times 10^5$	$8.21 \times 10^6$	$3.28 \times 10^6$	0.25	0.25	0.25
pvc	$25.0 \times 10^4$	$25.0 \times 10^4$	$25.0 \times 10^4$	$9.62 \times 10^4$	$9.62 \times 10^4$	$9.62 \times 10^4$	0.3	0.3	0.3
IM7	$163 \times 10^9$	$12 \times 10^9$	$12 \times 10^9$	$5 \times 10^9$	$4 \times 10^9$	$3.2 \times 10^9$	0.3	0.3	0.3

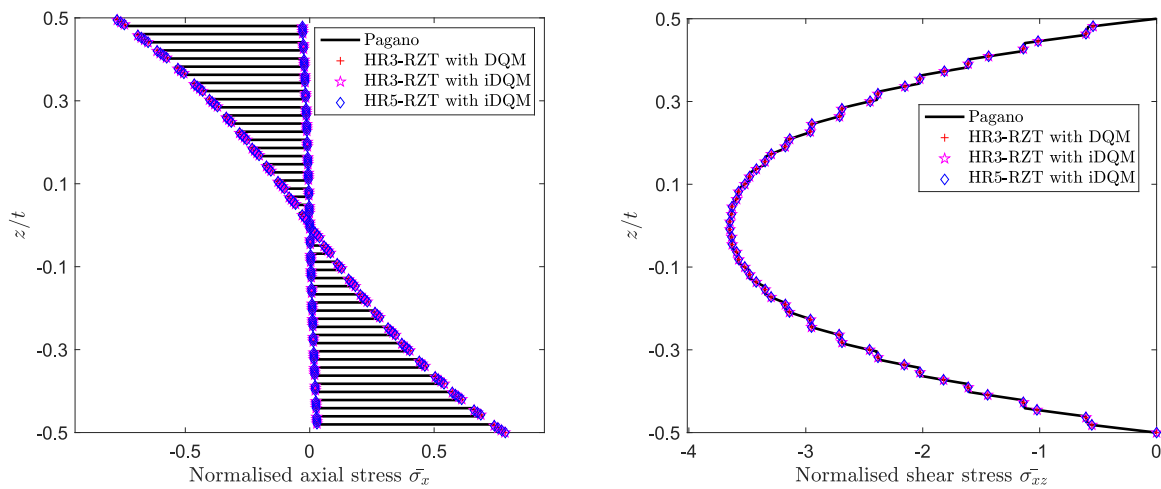
**Table 3**

Normalised maximum deflection, maximum axial stress and shear stress for simply-supported beams. Different results are specified by percentage errors in comparison with Pagano's solution.

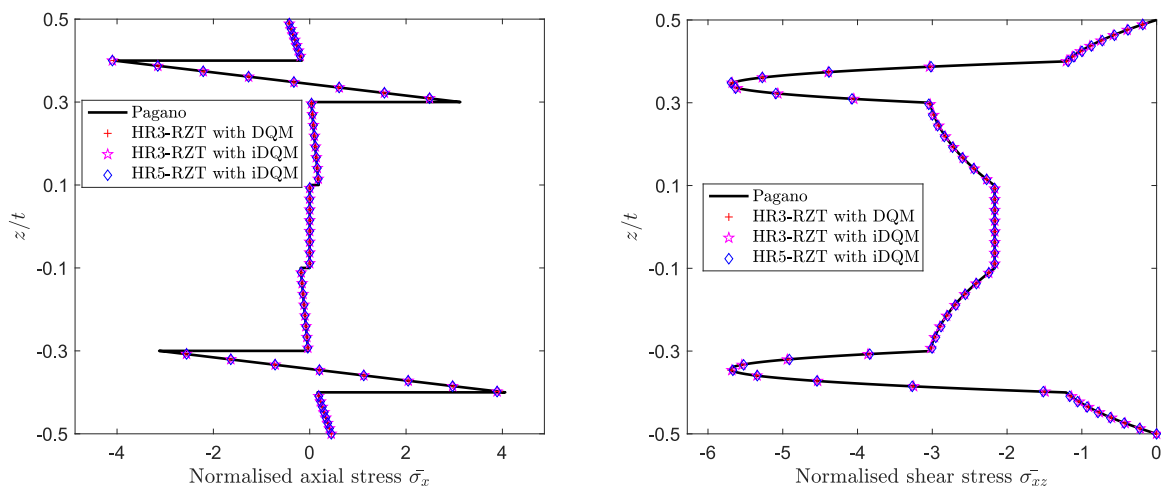
Laminate	Model	$\bar{w}$	$\bar{\sigma}_x^{max}$	$\bar{\tau}_{xz}^{max}$
SS <sub>1</sub>	Pagano	0.0303	1.6307	5.3340
	HR3-RZT with DQM	0.0303	(0.13) 1.6226	(−0.50) 5.3361
	HR3-RZT with iDQM	0.0304	(0.40) 1.6232	(−0.46) 5.3330
	HR5-RZT with iDQM	0.0304	(0.40) 1.6232	(−0.46) 5.3165
SS <sub>2</sub>	Pagano	0.0154	1.2239	3.6523
	HR3-RZT with DQM	0.0154	(0.14) 1.2280	(0.34) 3.6505
	HR3-RZT with iDQM	0.0155	(0.56) 1.2299	(0.49) 3.6484
	HR5-RZT with iDQM	0.0155	(0.56) 1.2322	(0.68) 3.6500
SS <sub>3</sub>	Pagano	0.4590	6.3417	5.6996
	HR3-RZT with DQM	0.4589	(−0.02) 6.3431	(0.02) 5.7014
	HR3-RZT with iDQM	0.4636	(0.99) 6.4016	(0.94) 5.7438
	HR5-RZT with iDQM	0.4636	(0.99) 6.4014	(0.94) 5.6973
SS <sub>4</sub>	Pagano	0.0100	0.9566	4.1236
	HR3-RZT with DQM	0.0100	(−0.03) 0.9526	(−0.42) 4.0903
	HR3-RZT with iDQM	0.0100	(0.34) 0.9513	(−0.55) 4.1050
	HR5-RZT with iDQM	0.0100	(0.34) 0.9456	(−1.15) 4.1040
SS <sub>5</sub>	Pagano	0.0115	1.0368	3.8037
	HR3-RZT with DQM	0.0115	(0.14) 1.0461	(0.90) 3.8026
	HR3-RZT with iDQM	0.0116	(0.49) 1.0473	(1.01) 3.7973
	HR5-RZT with iDQM	0.0116	(0.48) 1.0277	(−0.88) 3.8026



a. Laminate SS<sub>1</sub>



b. Laminate SS<sub>2</sub>



c. Laminate SS<sub>3</sub>

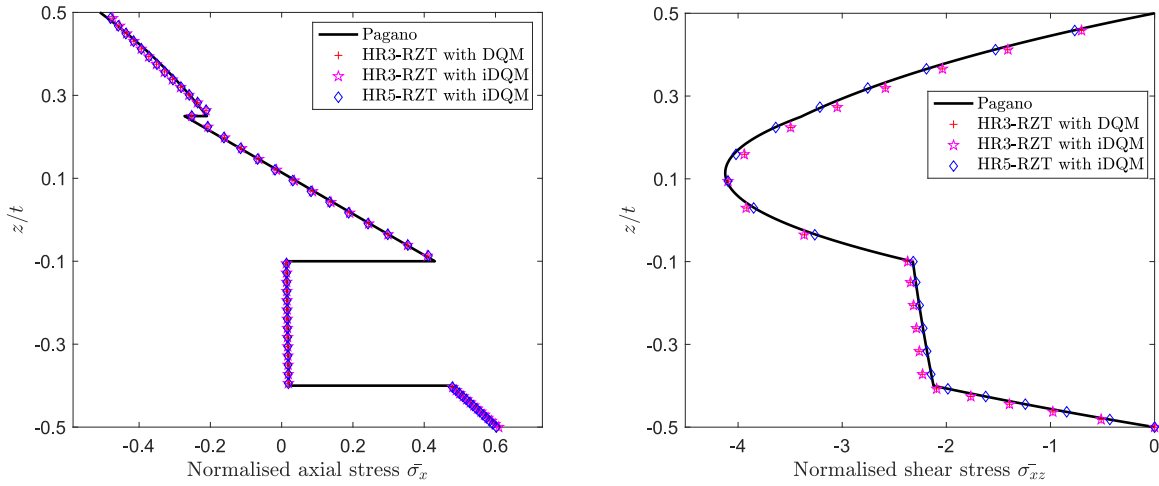
Fig. 3. Normalised axial and transverse shear stresses of symmetric laminates.

$$a_{ij}^{(1)} = l_k^{(1)}(x_j) = \begin{cases} \frac{1}{x_j - x_i} \prod_{k=1, k \neq i, j}^{N_p} \frac{x_j - x_k}{x_i - x_k} & \text{for } i \neq j \\ \prod_{k=1, k \neq i}^{N_p} \frac{1}{x_i - x_k} & \text{for } i = j \end{cases} \quad (43)$$

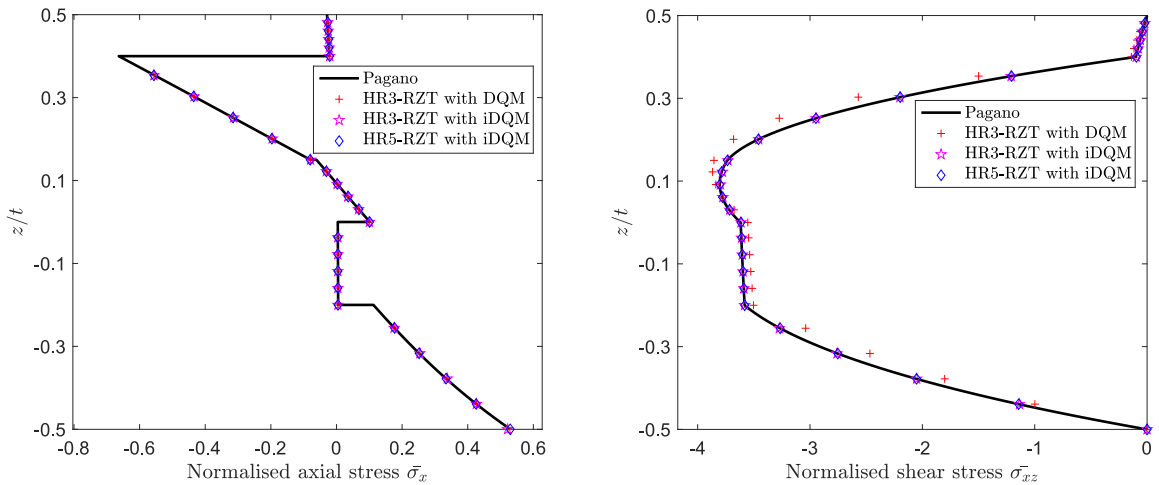
In a compact manner, Eq. (39) can be recast as

$$\mathbf{F}^{(1)} \approx \mathbf{D}^{(1)} \mathbf{F}, \quad (44)$$

where  $\mathbf{F}$  and  $\mathbf{F}^{(1)}$  are vectors of the function values and the first derivatives at grid points;  $\mathbf{D}^{(1)}$  is  $N_p \times N_p$  matrix of the first derivative weighting coefficients. Accordingly, the weighting coefficients for the  $n^{\text{th}}$  order derivatives are obtained by recursive formulae as



a. Laminate SS<sub>4</sub>



b. Laminate SS<sub>5</sub>

Fig. 4. Normalised axial and transverse shear stresses of asymmetric laminates.

Table 4  
Normalised axial stress, shear stress and maximum deflection for clamped beams.

Laminate	Model	0.25L			0.5L		
		$\bar{\sigma}_x^{min}$	$\bar{\sigma}_x^{max}$	$\bar{\tau}_{xz}^{max}$	$\bar{\sigma}_x^{min}$	$\bar{\sigma}_x^{max}$	$\bar{w}$
CC <sub>1</sub>	<b>3D Abaqus</b>	<b>-0.1612</b>	<b>0.1900</b>	<b>4.3170</b>	<b>-0.4836</b>	<b>0.5311</b>	<b>0.0088</b>
	HR3-RZT with DQM	-0.1743	0.1967	4.3062	-0.5065	0.5454	0.0089
	HR3-RZT with iDQM	-0.1627	0.1858	4.3088	-0.4949	0.5339	0.0088
	HR5-RZT with iDQM	-0.1650	0.1933	4.3089	-0.4985	0.5445	0.0088
CC <sub>2</sub>	<b>3D Abaqus</b>	<b>-0.2235</b>	<b>0.2593</b>	<b>3.2921</b>	<b>-0.5840</b>	<b>0.6328</b>	<b>0.0146</b>
	HR3-RZT with DQM	-0.2361	0.2619	3.2901	-0.6048	0.6415	0.0146
	HR3-RZT with iDQM	-0.2369	0.2609	3.2901	-0.6055	0.6406	0.0146
	HR5-RZT with iDQM	-0.2359	0.2589	3.2901	-0.6045	0.6386	0.0146

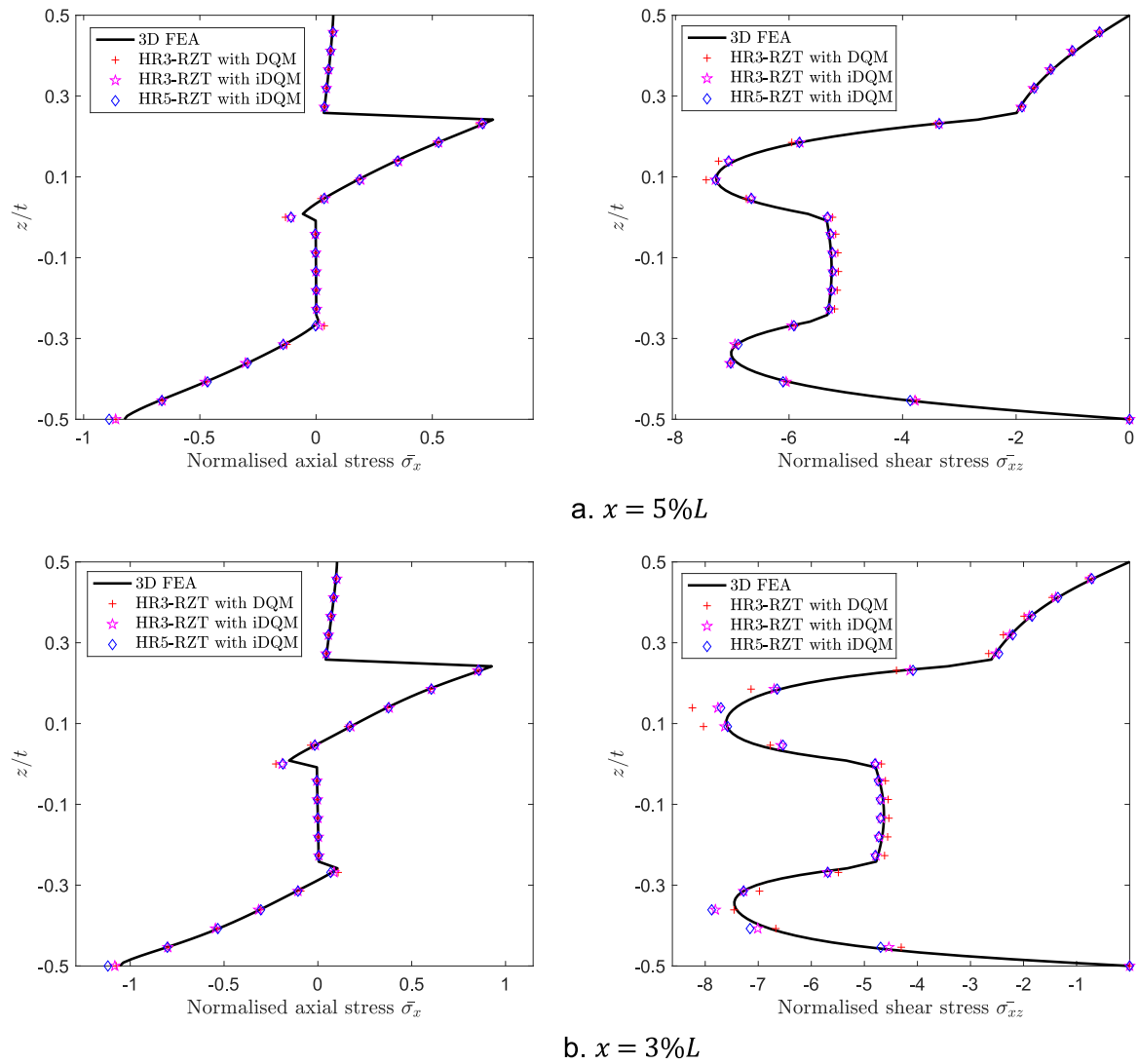


Fig. 5. Normalised axial and transverse shear stresses at the locations 5%, 3% of span from the left clamp (Laminate CC<sub>1</sub>).

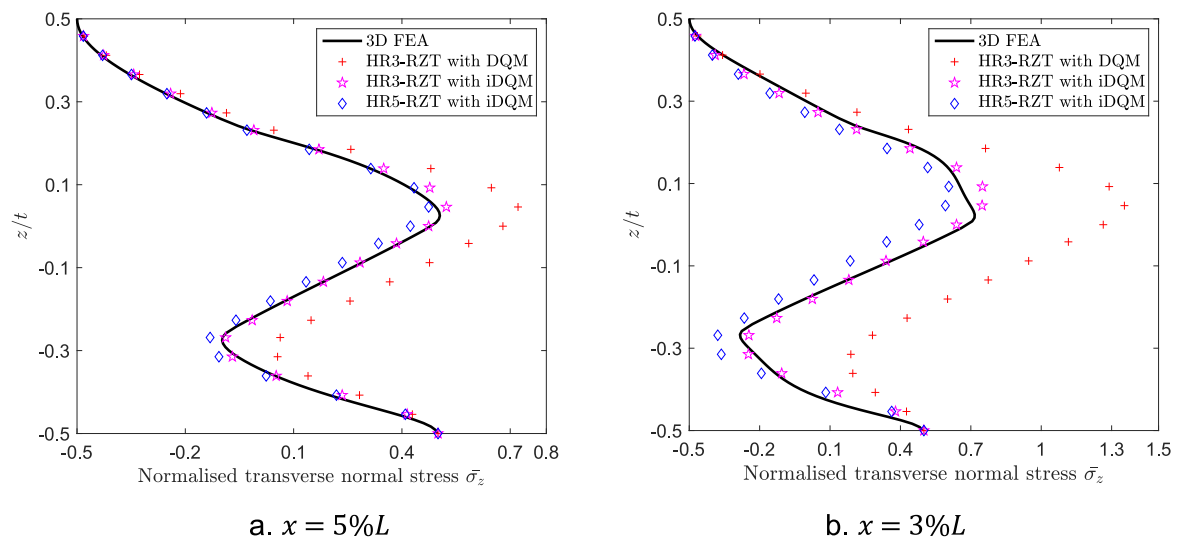


Fig. 6. Normalised transverse normal stress at the locations 5%, 3% of span from the left clamp (Laminate CC<sub>1</sub>).

$$\mathbf{F}^{(n)} \approx \mathbf{D}^{(n)} \mathbf{F}, \tag{45}$$

where  $\mathbf{D}^{(n)} = \mathbf{D}^{(1)} \mathbf{D}^{(n-1)}$  for  $n = 2, \bar{N}_p - 1$ . In the case of structural mechanics, both governing and boundary differential equations can be rewritten in algebraic form by replacing differential operators by the weighting coefficients in Eqs. (44) and (45). This procedure leads to a system of equations with unknowns being the functional values, e.g. displacements and stress resultants, at the grid points and can be readily solved by different numerical approaches.

2.4.2. Inverse differential quadrature method

In this section, a framework of inverse differential quadrature method is presented. Specifically, the Lagrange interpolation is implemented for the first derivative instead of the function itself. Higher-order derivative approximation is performed using the standard differentiation procedure of DQM with respect to the first-order derivative, whereas the functional values themselves are recovered by direct integration or as the inverse matrix of the first-derivative weighting coefficients.

Firstly, Lagrange interpolation  $l_k(x)$  is used to interpolate each function's first derivative as follows

$$f^{(1)}(x) \approx \sum_{j=1}^{N_p} l_k(x) f^{(1)}(x_j) \text{ for } j = 1, \bar{N}_p, \tag{46}$$

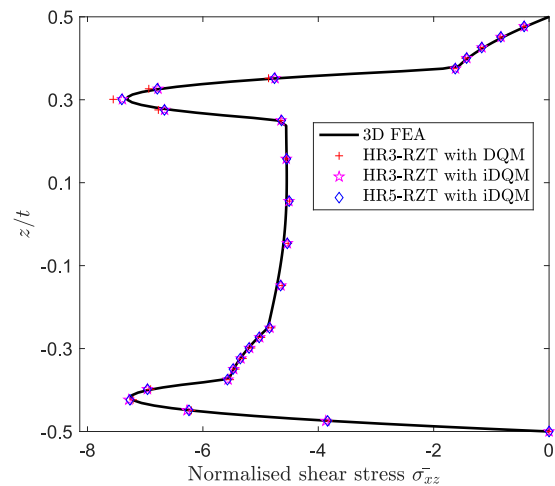
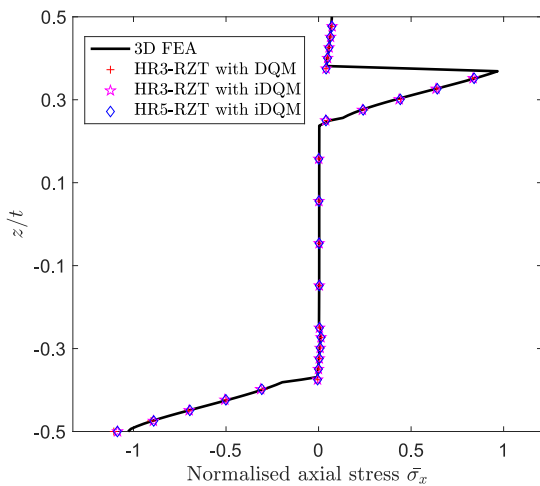
where  $f^{(1)}(x_j)$  is the first derivative of  $f(x)$  at  $N_p$  grid points  $x_j$ . The function is then obtained by integrating Eq. (46)

$$\begin{aligned} f(x) &= \int f^{(1)}(x) dx \approx \sum_{j=1}^{N_p} f^{(1)}(x_j) \int l_k(x) dx + c_1 \\ &= \sum_{j=1}^{N_p} I_k^{[1]}(x) f^{(1)}(x_j) + c_1, \end{aligned} \tag{47}$$

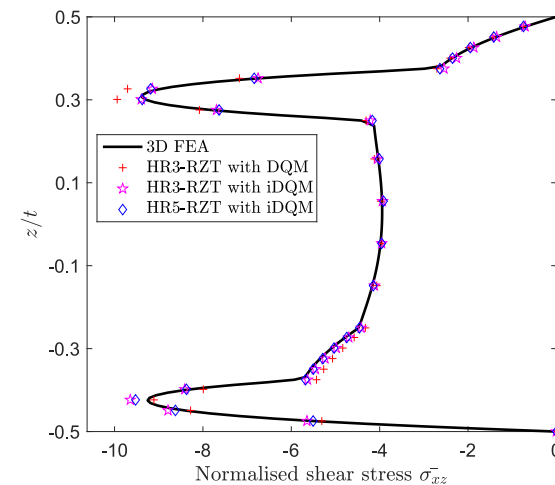
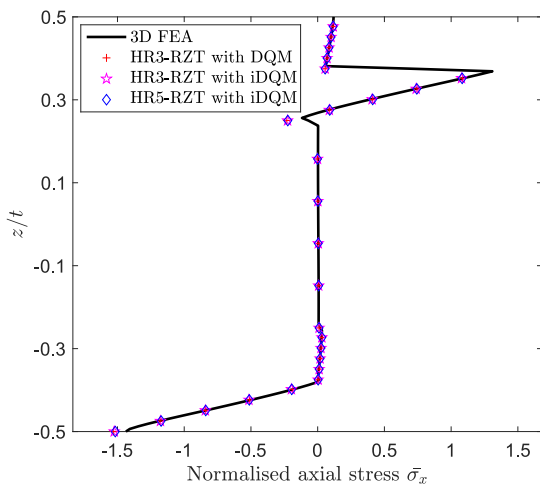
where  $I_k^{[1]}(x) = \int l_k(x) dx$ ,  $c_1$  is the integration constant and superscript in bracket  $[\cdot]$  denotes the order of integration. Using  $N_p$  grid points, the Lagrange interpolation is of order  $N_p - 1$  hence  $I_k^{[1]}(x)$  is an  $N_p$ -order function. Eq. (47) can be rewritten in a compact form as

$$\mathbf{F} \approx \mathbf{I}^{[1]} \mathbf{F}^{(1)} + \mathbf{I} c_1 = \hat{\mathbf{I}}^{[1]} \hat{\mathbf{F}}^{(1)}, \tag{48}$$

where  $\mathbf{F}$  and  $\mathbf{F}^{(1)}$  are vectors of function values and first derivatives at grid points, respectively;  $\hat{\mathbf{I}}^{[1]}$  is a  $N_p \times N_p$  matrix of weighting integration coefficients and  $\mathbf{I}$  is a unit column vector containing  $N_p$



a.  $x = 5\%L$



b.  $x = 3\%L$

Fig. 7. Normalised axial and transverse shear stresses at the locations 5%, 3% of span from the left clamp (Laminate CC<sub>2</sub>).

entries;  $\hat{\mathbf{I}}^{[1]} = [\mathbf{I}^{[1]} \quad \mathbf{I}]$  is a  $N_p \times (N_p + 1)$  matrix; and  $\hat{\mathbf{F}}^{(1)} = [\mathbf{F}^{(1)} \quad c_1]^T$  is a  $N_p + 1$  column vector. As can be observed in Fig. 2, analytical integration for  $I_k^{(1)}(x)$  becomes cumbersome and computationally expensive as  $N_p$  increases. In this figure, the computing times are obtained for the same laptop with Intel Core i7-8565U, RAM 8 GB using iteration over the change of number of grid points. The following step presents a remedy for this deficiency, where matrix  $\mathbf{I}^{[1]}$  can be obtained by inversion of the first derivative matrix  $\mathbf{D}^{(1)}$ . To diminish numerical error and establish an equivalent platform of computational inversion for  $\mathbf{I}^{[1]}$ , the approximation in Eq. (44) can be expressed in equality form by including error estimation for the first order numerical differentiation as

$$\mathbf{F}^{(1)} = \mathbf{D}^{(1)}\mathbf{F} + \mathbf{E}^{(1)}, \quad (49)$$

where  $\mathbf{E}^{(1)}$  is the vector of error values for the first derivatives at grid points using the Lagrange polynomial interpolation. Left-multiplying Eq. (49) by the inversion of  $\mathbf{D}^{(1)}$  leads to the expression of function values from their first derivatives as follows

$$\begin{aligned} \mathbf{F} &= [\mathbf{D}^{(1)}]^{-1}\mathbf{F}^{(1)} - [\mathbf{D}^{(1)}]^{-1}\mathbf{E}^{(1)} = \tilde{\mathbf{I}}^{[1]}\mathbf{F}^{(1)} - \tilde{\mathbf{I}}^{[1]}\mathbf{E}^{(1)} \\ &= \tilde{\mathbf{I}}^{[1]}\mathbf{F}^{(1)} + \mathbf{I}\bar{c}_1, \end{aligned} \quad (50)$$

where  $\tilde{\mathbf{I}}^{[1]} = [\mathbf{D}^{(1)}]^{-1}$ , and  $\mathbf{I}\bar{c}_1 = -\tilde{\mathbf{I}}^{[1]}\mathbf{E}^{(1)}$  is the average error distributed over all grid points.

Let us consider a domain  $[0, L]$  as is usually illustrated for a one-dimensional beam problem. Evaluating the function at  $x_0 = 0$  using Eq. (48) and (50), as  $I_{(k)}(0) = 0$  according to Eq. (41), then

$$\bar{c}_1 = c_1 - \tilde{\mathbf{I}}^{[1]}(0)\mathbf{F}^{(1)}, \quad (51)$$

where  $\tilde{\mathbf{I}}^{[1]}(0)$  is a row vector of  $\tilde{\mathbf{I}}^{[1]}$  associated with  $x_0 = 0$ , i.e. the first row in the domain  $[0, L]$ .

Substituting Eq. (51) into Eq. (50) gives a new form of function approximation based on its derivatives as follows

$$\mathbf{F} = [\tilde{\mathbf{I}}^{[1]} - \mathbf{I}\tilde{\mathbf{I}}^{[1]}(0)]\mathbf{F}^{(1)} + \mathbf{I}c_1. \quad (52)$$

Comparing Eqs. (52) and (48), the relation between integration and differentiation weighting coefficients can be established as

$$\mathbf{I}^{[1]} = \tilde{\mathbf{I}}^{[1]} - \mathbf{I}\tilde{\mathbf{I}}^{[1]}(0) = [\mathbf{D}^{(1)}]^{-1} - \mathbf{I}[\mathbf{D}^{(1)}]^{-1}(0). \quad (53)$$

For the standard DQM approach, the differential governing Eq. (35) and boundary Eq. (37) are converted to algebraic equations using the approximations in Eqs. (44) and (45). This results in the unknowns being the stress resultant  $\mathcal{F}$  and Lagrange multipliers  $\lambda_1$  and  $\lambda_2$ . It is worth mentioning that the governing equation Eqs. (35c) and (37a) are of fourth- and third- order, respectively, and computation of the shear Eq. (14) and transverse normal stress Eq. (18) involves first- and second-order differentiation. Meanwhile, for the iDQM approach, the unknowns are the Lagrange multipliers and the first derivatives of  $\mathcal{F}$ , thereby reducing the order of differentiation in both governing and boundary equations by one. In other words, Eqs. (35) and (37) can be rewritten with respect to the first derivatives of stress resultants, i.e.,  $\mathbf{F}^{(1)} = \partial\mathcal{F}/\partial x$ , in which  $\mathbf{F}^{(1)}$  contains seven components denoted by  $\mathbf{F}_i^{(1)}$  ( $i = \overline{1-7}$ ) as follows

$$\delta\lambda_1 : \mathbf{F}_1^{(1)} + \hat{T}_t - \hat{T}_b = 0, \quad (54a)$$

$$\delta\lambda_2 : \mathbf{F}_{2,x}^{(1)} + Z_N\hat{T}_{t,x} - Z_0\hat{T}_{b,x} + \hat{P}_t - \hat{P}_b = 0, \quad (54b)$$

$$\begin{aligned} \delta\hat{\mathbf{I}}^{[1]}\hat{\mathbf{F}}^{(1)} : \mathbf{s}^T\hat{\mathbf{I}}^{[1]}\hat{\mathbf{F}}^{(1)} - (\boldsymbol{\eta} - \boldsymbol{\omega})^T\hat{\mathbf{F}}_x^{(1)} + \boldsymbol{\rho}^T\hat{\mathbf{F}}_{,xxx}^{(1)} \\ \delta\hat{\mathbf{I}}^{[1]}\hat{\mathbf{F}}^{(1)} : \mathbf{s}^T\hat{\mathbf{I}}^{[1]}\hat{\mathbf{F}}^{(1)} - (\boldsymbol{\eta} - \boldsymbol{\omega})^T\hat{\mathbf{F}}_x^{(1)} + \boldsymbol{\rho}^T\hat{\mathbf{F}}_{,xxx}^{(1)} + \frac{\boldsymbol{\omega}_b^T}{2}\hat{P}_b + \boldsymbol{\rho}_p^T\hat{P}_{b,xx} \\ - \left(\mathbf{i} + \frac{\boldsymbol{\omega}_t}{2}\right)^T\hat{T}_{b,x} - \boldsymbol{\rho}_t^T\hat{T}_{b,xxx} + \boldsymbol{\Lambda}_{eq} \\ = 0 \end{aligned} \quad (54c)$$

and

$$\begin{aligned} \delta\hat{\mathbf{I}}^{[1]}\hat{\mathbf{F}}^{(1)} = 0 \text{ or } \left(\boldsymbol{\eta} - \frac{\boldsymbol{\omega}}{2}\right)^T\hat{\mathbf{F}}^{(1)} - \boldsymbol{\rho}^T\hat{\mathbf{F}}_{,xx}^{(1)} - \mathbf{i}^T\hat{T}_b + \boldsymbol{\rho}_t^T\hat{T}_{b,xx} \\ - \boldsymbol{\rho}_p^T\hat{P}_{b,x} + \boldsymbol{\Lambda}_{bc_1} \\ = \hat{U} \end{aligned} \quad (55a)$$

$$\delta\hat{\mathbf{F}}^{(1)} = 0 \text{ or } \frac{\boldsymbol{\omega}^T}{2}\hat{\mathbf{I}}^{[1]}\hat{\mathbf{F}}^{(1)} + \boldsymbol{\rho}^T\hat{\mathbf{F}}_x^{(1)} - \boldsymbol{\rho}_t^T\hat{T}_{b,x} + \boldsymbol{\rho}_p^T\hat{P}_b + \boldsymbol{\Lambda}_{bc_2} = \hat{V} \quad (55b)$$

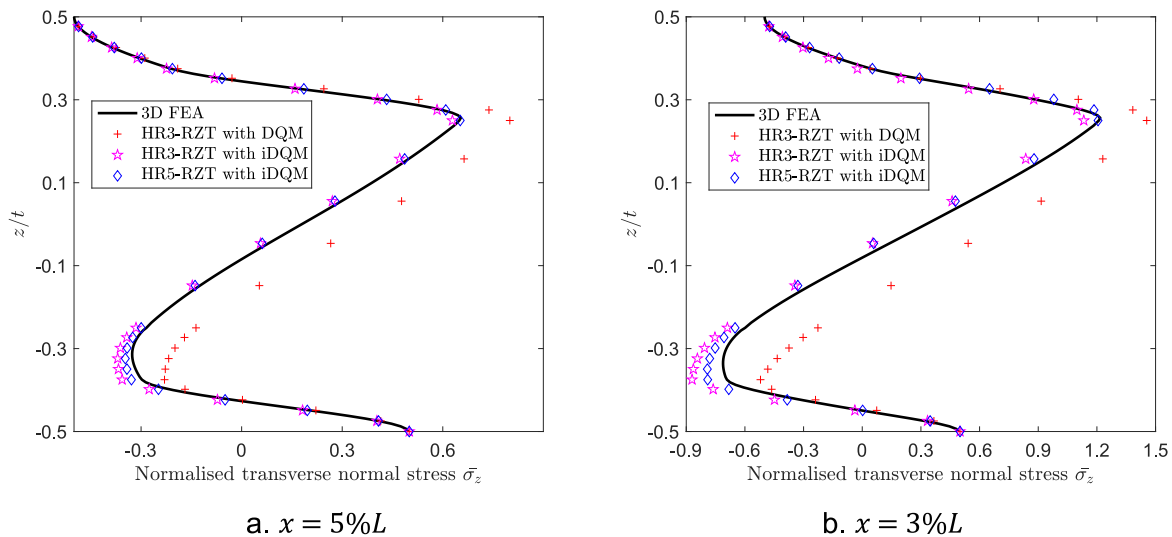


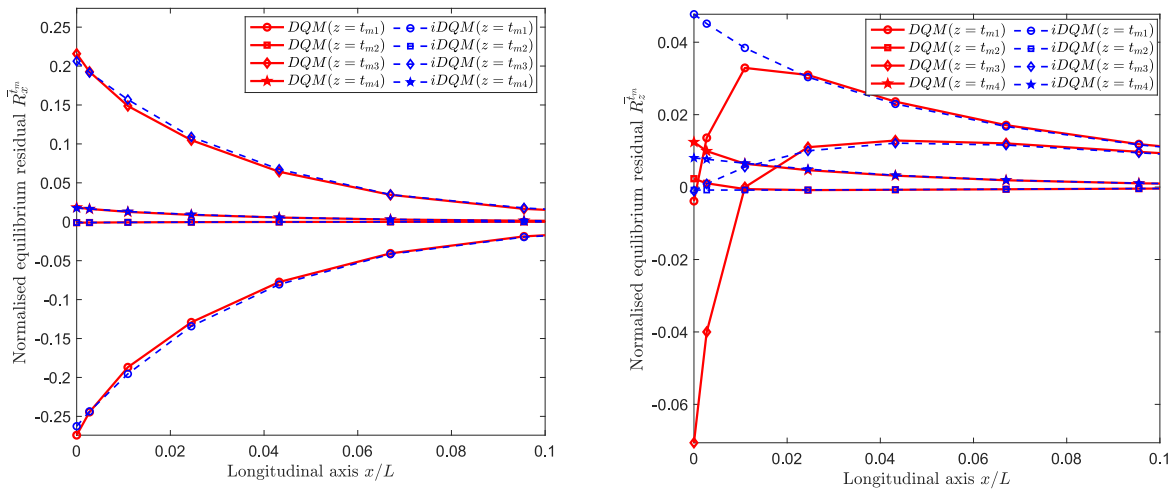
Fig. 8. Normalised transverse normal stress at the locations 5%, 3% of span from the left clamp (Laminate CC<sub>2</sub>).

### 3. Numerical results and discussions

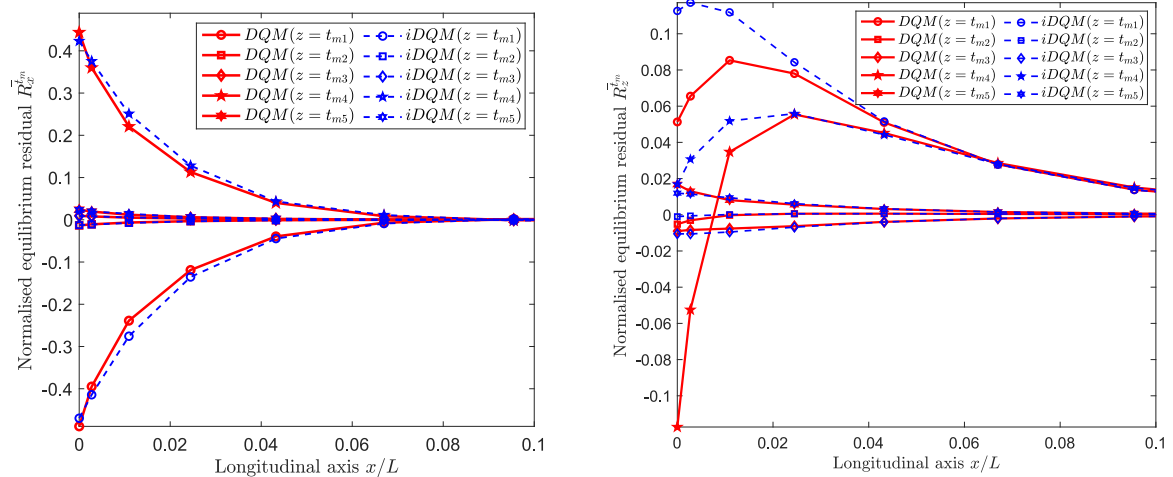
In this section, examples of flexural analysis for various laminated beams under different boundary conditions are presented. These examples include a validation against Pagano’s exact solution for simply-supported constant stiffness beams, followed by the investigation of localised stresses near clamped ends in Section 3.1. Efficiency of the inverse differential quadrature method (iDQM) and its implementation for a third-order and a fifth-order refined zigzag theory (HR3-RZT and HR5-RZT), which are based

on the Hellinger-Reissner (HR) variational principle, are discussed. Furthermore, bending behaviour of variable angle tow (VAT) beams is considered in Section 3.2 by employing the iDQM solution with Murakami zigzag function (MZZF). For verification purposes, the vertical displacement, normal stress, transverse shear stress and transverse normal stress are normalised as follows:

$$\bar{w} = \frac{10^6 t^3}{q_0 L^4} u_z, \bar{\sigma}_x = \frac{t^2}{q_0 L^2} \sigma_x, \bar{\tau}_{xz} = \frac{\tau_{xz}}{q_0}, \bar{\sigma}_z = \frac{\sigma_z}{q_0}. \tag{56}$$



a. Laminate CC<sub>1</sub>



b. Laminate CC<sub>2</sub>

Fig. 9. Normalised equilibrium residual for clamped beams.

Table 5  
Normalised axial stress, shear stress and maximum deflection for cantilevered beam (Laminate CF).

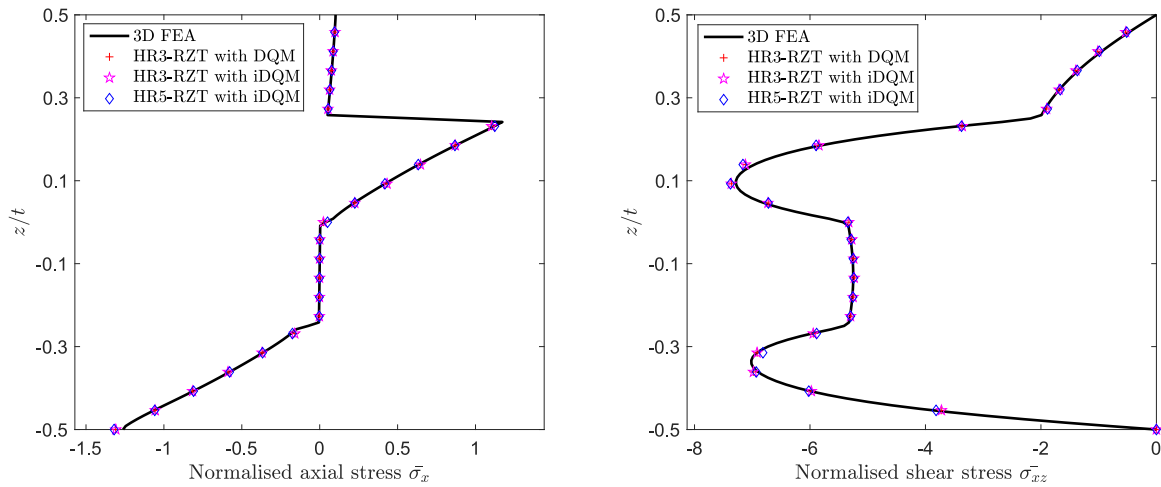
Model	0.25L			Tip $\bar{w}(L)$
	$\bar{\sigma}_x^{\min}$	$\bar{\sigma}_x^{\max}$	$\bar{\tau}_{xz}^{\max}$	
<b>3D Abaqus</b>		<b>0.7110</b>	<b>5.9131</b>	<b>0.2364</b>
HR3-RZT with DQM	-0.7576	0.7243	5.9598	0.2371
HR3-RZT with iDQM	-0.7574	0.7243	5.9609	0.2347
HR5-RZT with iDQM	-0.7572	0.7320	5.9160	0.2347

3.1. Constant stiffness laminated beams

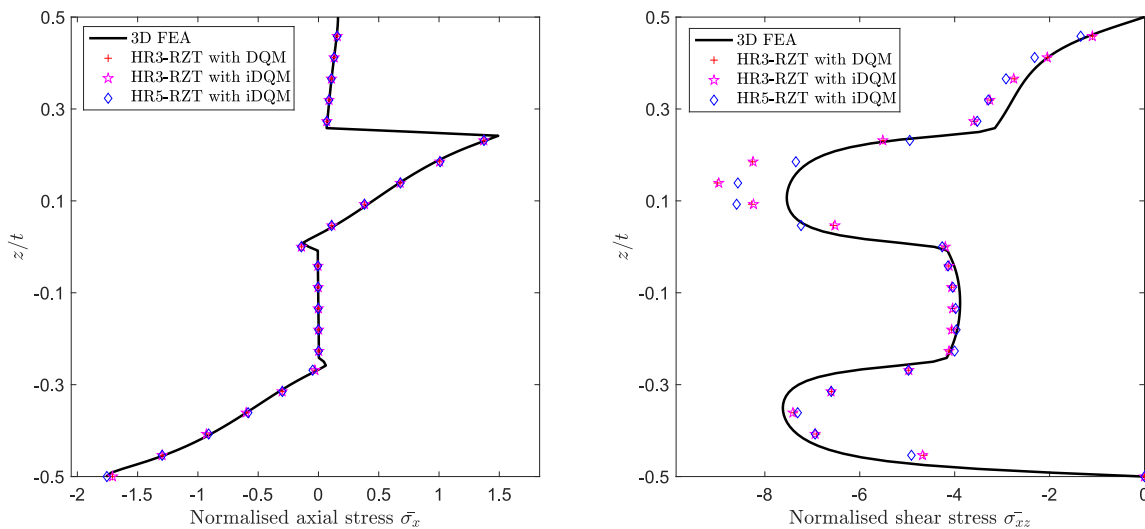
3.1.1. Simply supported beams with constant stiffness composites

The first example considers a simply supported beam composed of different layups and materials. The beam is comparatively thick with length-to-thickness ratio  $L/t = 8$ . The plane strain condition is invoked in the beam's width direction, i.e. the beam is assumed to be infinitely wide. To compare with the analytical 3D solutions by (Pagano, 1969), a sinusoidal distributed load is considered. It is worth noting that, as a benchmark for equivalent single layer solution (ESL) for beams, (Groh and Weaver, 2015) split the load into top and bottom surface pressures,  $\hat{P}_t = \hat{P}_b = -q_0/2\sin(\pi x/L)$ . This load profile is also used here for verification purposes. In the present work, computational performance has been investigated for all beam configurations previously considered in Refs. (Groh and Weaver, 2015; Patni et al., 2018; Trinh et al., 2020) and excellent agreements are observed throughout. However, only a set of three symmetric and two asymmetric laminated beams with layup properties presented in Table 1 are discussed currently for a concise presentation. Material properties for all beams investigated in this

paper are presented in Table 2. As presented in (Groh and Weaver, 2015), material  $p$  is a representative of a carbon-fibre reinforced plastic while material  $m$  features an increased transverse stiffness. Material  $h$  is a transversely isotropic honeycomb tailored to a significantly lower shear stiffness compared with material  $p$ . Finally, material  $pvc$  is an isotropic closed-cell poly-vinyl chloride foam. For symmetric layups, a ply-constant-thickness beam ( $SS_1$ ) with Externally Weak Layers (Gherlone, 2013) and a 51 alternative cross-ply beam ( $SS_2$ ) together with a multi-material sandwich beam ( $SS_3$ ) are considered. For antisymmetric beams, laminates constituted of materials  $p$  and  $m$  with an approximately 10% shift up of the neutral axis are investigated. Table 3 shows comparative results of the present iDQM-based HR3-RZT and HR5-RZT solutions against the exact solution reported by (Pagano, 1969) and a DQM-based HR3-RZT solution developed by (Groh and Weaver, 2015). It is observed that the accuracy of iDQM-based solutions for maximum deflection, axial stress at the middle of the beam and shear stress at the supported ends is within 1.15% in comparison with the 3D exact solution. Further demonstration of through-thickness stresses is presented in Figs. 3 and 4. It is noted that axial



a.  $x = 10\%L$



b.  $x = 3\%L$

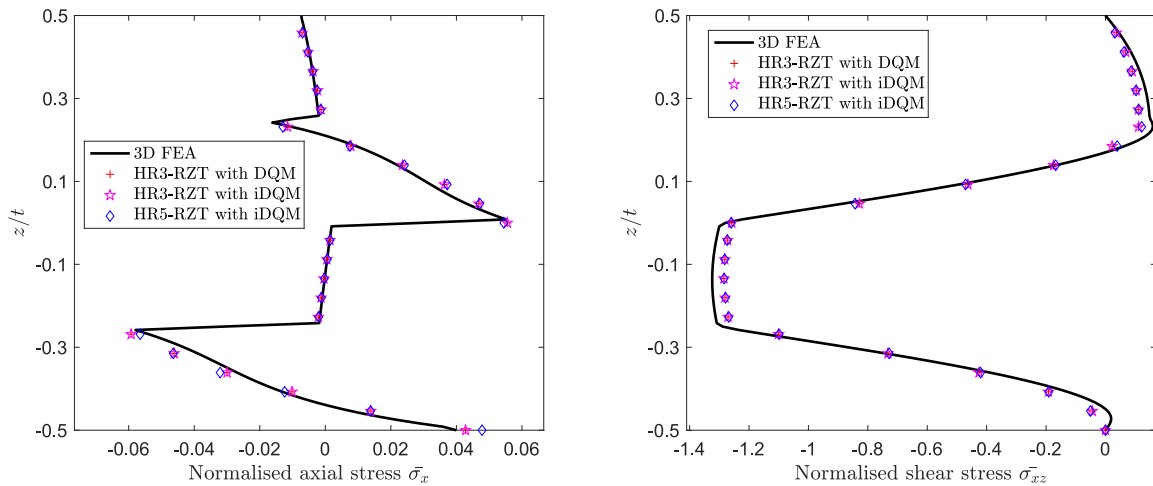
Fig. 10. Normalised axial and transverse shear stresses near the clamped end (Laminate CF).

stress of both DQM and iDQM solutions match perfectly with the exact solution at the middle of all symmetric and non-symmetric beams. With respect to the shear stress at 1% of the beam’s span (almost at the support), slight improvements by the iDQM solutions are observed for non-symmetric beams compared to the DQM solution. More specifically, the improvement of accuracy for shear stress in laminate  $SS_4$  comes from a finer kinematics assumption (fifth-order axial displacement in HR5-RZT compared with a third-order in HR3-RZT), but the improvement in laminate  $SS_5$  may come from the iDQM solution as more accurate shear stress is observed in both iDQM-based HR3-RZT and HR5-RZT solutions.

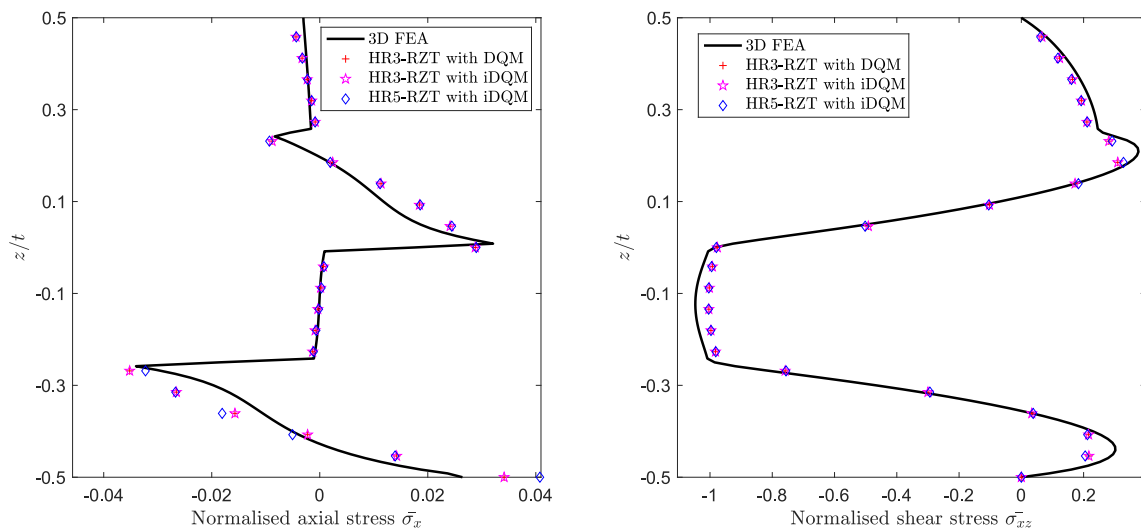
3.1.2. Clamped and cantilevered beams with constant stiffness composites

Further validation of the proposed iDQM solutions for cantilevered and clamped beams under uniformly distributed load is presented in this section with more attention placed on the localised stress profiles near the boundaries. For the clamped beams, moderate thick ( $L/t = 10$ ) anti-symmetric and sandwiched beams

are analysed. This example is conducted for anti-symmetric cross-ply beams and sandwich beams, in which the layup configurations are described in Table 1. For validation, an Abaqus model is made and the DQM solution (Groh, 2015; Groh et al., 2015) is used to generate reference data. Following the approach described in (Groh, 2015; Groh et al., 2015), a 3D Abaqus model with 799 C3D8R elements along the beam axis and 120 elements in the thickness direction are used. To enforce the plane strain condition, the width dimension is set at a high value compared to the axial and thickness dimensions. Table 4 presents the maximum axial stress, shear stress and deflection at position  $x = 25\%L$  and at the middle of the beam  $x = 50\%L$ . Additionally, detailed through-thickness stress components near the beam ends are presented in Figs. 5–8. While the global behaviours, i.e. maximum deflection and stresses far from the boundaries, are similar for all the ESL solutions in comparison with the 3D Abaqus solution, improvements are observed in iDQM solutions for localised stresses near the clamped supports. In fact, approaching the left clamp ( $x = 0$ ) from positions  $x = 5\%L$  to  $x = 3\%L$ , the transverse shear and normal stresses predicted by both iDQM models agree with the



a.  $x = 90\%L$  (near the free end on the right of the beam)



b.  $x = 95\%L$  (near the free end on the right of the beam)

Fig. 11. Normalised axial and transverse shear stresses near the free end (Laminate CF).

Abaqus solution better than those by the DQM solution for both considered laminates. Interestingly, up to 3% of the span from the clamped supports, the transverse normal stress from the iDQM solutions agrees well with the 3D solution although significant deviations for the DQM-based solution is observed. As an additional way of demonstrating the efficiency of iDQM solutions, Cauchy's equilibrium is examined for points along the beam. The residuals of longitudinal and transverse equilibria are normalised with respect to the load magnitude  $q_0$  according to the relation

$$\bar{R}^{t_{m_i}} = \frac{1}{q_0}(\sigma_{x,x} + \sigma_{xz,z}); \bar{R}_z^{-t_{m_i}} = \frac{1}{q_0}(\sigma_{xz,x} + \sigma_{z,z}). \tag{57}$$

In these residuals, differentiation with respect to the  $x$ -axis is computed directly from the differential matrix in the DQM formulation (i.e., Eq. (44)) whilst differentiation with respect to the  $z$ -axis is calculated using the *gradient* function in MATLAB. Equilibrium is assessed for points located in the middle of each ply through the thickness ( $z = t_m$ ). The residuals are plotted in Fig. 9 for 10% of

the span from the left clamp. It is worth noting that based on the HR3-RZT formulation, governing and boundary equations are identical for DQM and iDQM solutions. Therefore, the deviation observed in Fig. 9 is basically produced by the approximating approaches, i.e., the primary unknowns in the DQM are the force and moments while their derivatives are the primary unknowns

in iDQM. It is observed that  $\bar{R}_x^{-t_{m_i}}$  is almost the same for both solutions, with a small enhancement in iDQM near the clamped end. More improvement is shown in  $\bar{R}_z^{-t_{m_i}}$ , which could be responsible for the better prediction of the iDQM solution of the transverse shear and normal stresses near the boundary. This is an observation demonstrating the efficiency of the iDQM solution for multifunctional approximation, corroborating the iDQM error analysis described in (Ojo et al., 2020).

For a cantilevered case, a thick beam ( $L/t = 5$ ) with anti-symmetric layup clamped on the left end ( $x = 0$ ) and free at the other end ( $x = L$ ) is considered. The tip deflection and stress components at position  $x = 25\%L$  are presented in Table 5. Further

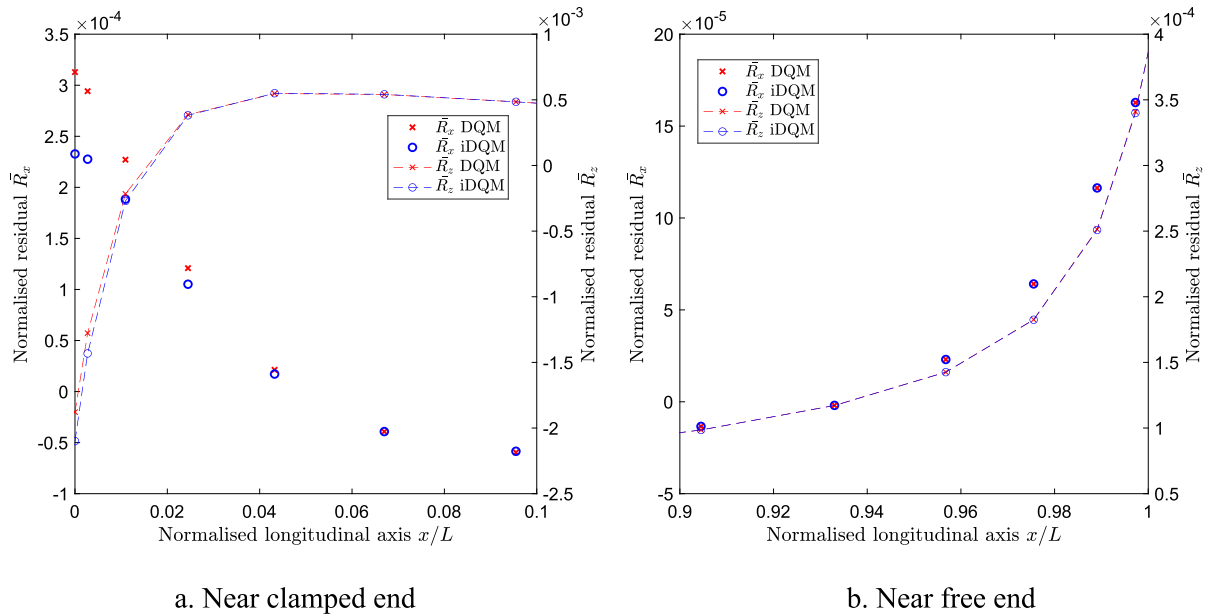


Fig. 12. Normalised equilibrium residual for cantilevered beam (Laminate CF).

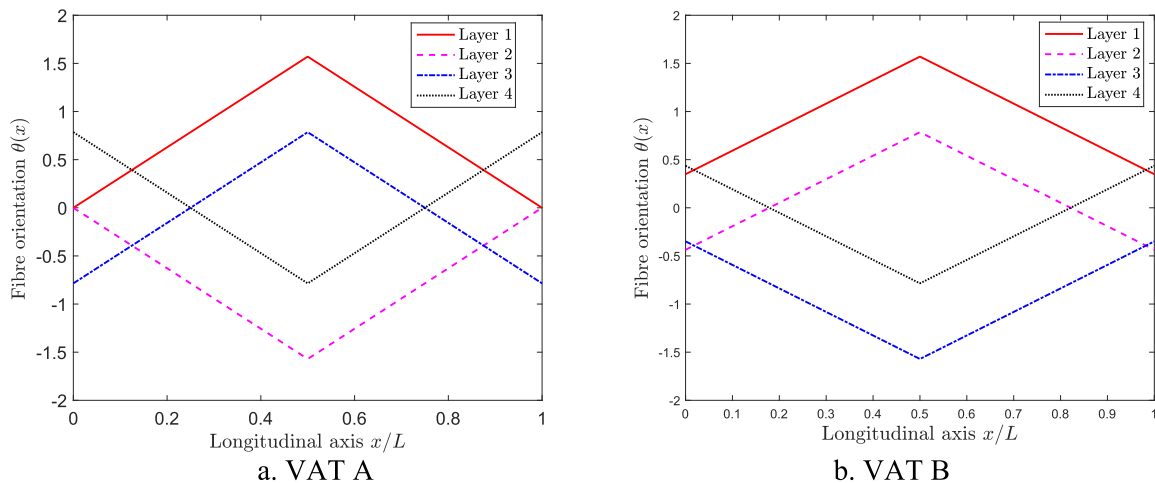


Fig. 13. Fibre orientation along the beam axis (VATs A and B). These plots are for below half of the thickness due to symmetry.

details of thickness-wise stress distributions near the clamped and free ends are depicted in Figs. 10 and 11. For this cantilevered beam, all the ESL solutions based on DQM and iDQM provide the same level of accuracy for stresses compared with the 3D Abaqus solution. In other words, there is no significant improvement in either numerical method or the kinematics chosen. The observed discrepancy between ESL and 3D solutions at position  $x = 3\%L$  near the clamped end is due to boundary effects.

The axial stress near the free end changes sign within each ply confirming a strong zigzag effect in this area. Moreover, from the axial stress profile, higher zigzag kinematics corresponding to local stress-channelling within each ply is probably required to capture the stress fields near the free end. With respect to computational solutions, a plot of equilibrium residuals near the clamped and the free ends is presented in Fig. 12. The residuals in this figure

**Table 6**

Stacking sequence for VAT beams.  $(T_0|T_1)$  indicates the fibre angle at the middle and the ends of beams, respectively.

VAT	Stacking sequence
A	$[(90 0)/(-90 0)/(45 -45)/(-45 45)]_s$
B	$[(90 20)/(45 -25)/(-90 -20)/(-45 25)]_s$

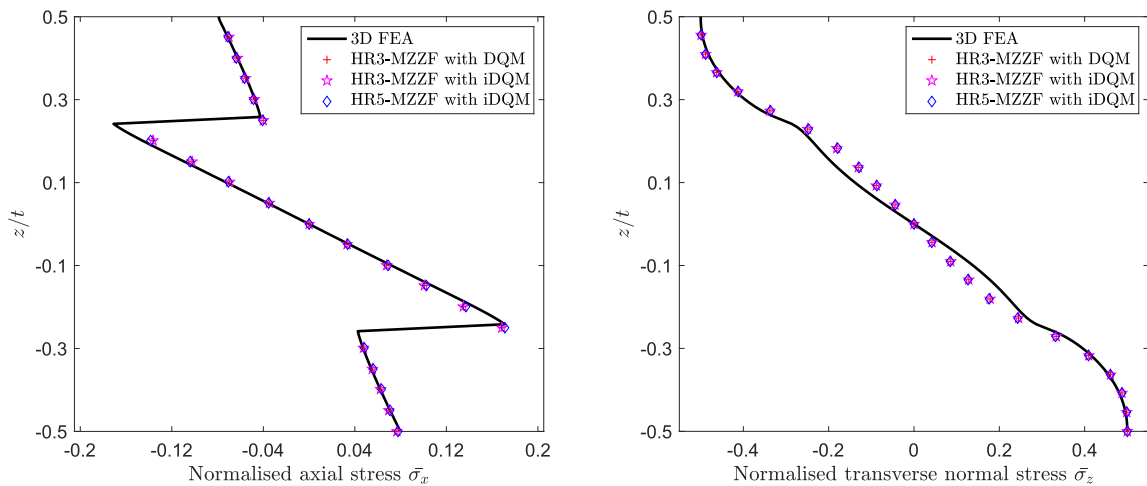
are computed by integrating the residuals in Eq. (57) through thickness as follows

$$\bar{R}_x = \frac{1}{q_0} \int_{-t/2}^{t/2} (\sigma_{x,x} + \sigma_{xz,z}) dz; \bar{R}_z = \frac{1}{q_0} \int_{-t/2}^{t/2} (\sigma_{xz,x} + \sigma_{z,z}) dz. \quad (58)$$

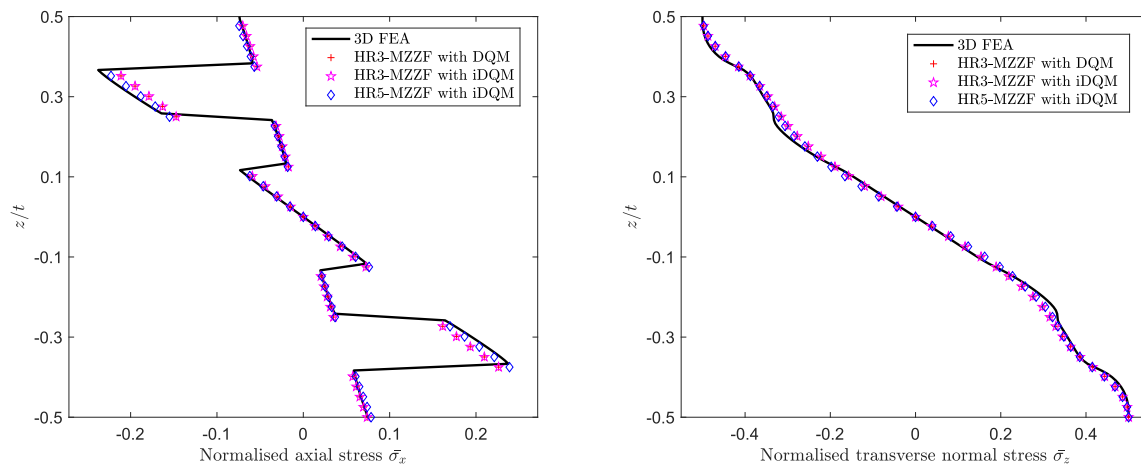
These residuals are associated with thickness-wise average errors of the ESL concept, which can be used to measure the accuracy of DQM and iDQM solutions for the same set of governing and boundary equations based on HR3-RZT. It is observed that Cauchy's equilibrium is satisfied up to the same level of accuracy near both the clamped and free ends. This observation corroborates the similar accuracy between the DQM and iDQM for the corresponding stress prediction. A possible explanation for the lack of improvement of iDQM over DQM in this case is that the variation of stress resultants and displacement functionals along the beam axis is slow; similar to the simply supported beam but contrary to the doubly clamped beam; hence, little numerical error is induced by differentiation.

### 3.2. Variable angle tow (VAT) laminated beams

In this section, validation of iDQM solutions is performed for VAT composite beams, i.e. beams comprised of composite laminae



a. VAT A



b. VAT B

**Fig. 14.** Normalised axial and transverse normal stresses at the middle of the beam (VATs A and B).

where the fibre angles with each lamina vary spatially along the length of the beam. The fibre orientation is assumed to vary linearly along the spanwise direction and constant through the thickness of each lamina. The fibre orientation is defined using the relation given by (Gürdal and Olmedo, 1993) as follows

$$\theta^{(k)}(x) = \frac{2(T_1^{(k)} - T_0^{(k)})}{L} \left| x - \frac{L}{2} \right| + T_0^{(k)}, \quad (57)$$

where  $\theta^{(k)}(x)$  is the fibre angle at position  $x$ ,  $T_0^{(k)}$  and  $T_1^{(k)}$  denoted by  $\langle T_0^{(k)} | T_1^{(k)} \rangle$  are the angles at the mid-span and at the beam's ends, respectively. By this definition, the fibre angle in layer ( $k$ ) takes the value of  $T_0^{(k)}$  at the mid-span and varies linearly towards  $T_1^{(k)}$  at both ends. It is worth mentioning that, the material is defined as a function of  $x$  in both DQM and iDQM solutions, that is,  $\theta^{(k)}(x)$  is calculated at every grid point which is used to approximate the field functionals and material constants are computed corresponding to  $\theta^{(k)}(x)$ . Two stacking sequences tabulated in Table 1 made of IM7/8552 epoxy resin, a carbon-fibre reinforced plastic material commonly used in industry, are considered (denoted by IM7 in material property tables). The fibre orientation variation for these laminates is plotted in Fig. 13. As discussed in (Groh, 2015; Groh et al., 2015; Patni et al., 2019), Murakami's zigzag function provides

a more stable solution for stress analysis of VAT laminates due to the non-existence of shear modulus derivatives, which can cause computational issues in ESL models based on the refined zigzag theory. Therefore, the Murakami zigzag function is used in this section in combination with a global through-thickness third-order and fifth-order kinematics in the framework of HR mixed variational formulation. The outputs from these models are denoted by HR3-MZZF and HR5-MZZF, respectively.

Deflection and stresses at specific positions are presented for moderately thick clamped beams ( $L/t = 10$ ) in Table 6 and the variations of stresses towards the left clamped end are plotted in Figs. 14–16. Although both VAT beams comprise eight equal-thickness layers, VAT A behaves as a three-ply beam due to the symmetry of each two consecutive layers with a double thickness in the middle layer. From the stress profile in the middle of the beams (Fig. 14), the DQM and iDQM solutions provide the same accuracy of stress prediction in the middle of the beams and higher-order kinematics, i.e. HR5-MZZF, improve the accuracy of the HR model compared to the HR3-MZZF model. This observation is more pronounced towards the clamped ends where the variation of stress and displacement fields are more rapid. Two different sources of improvement in predicting the axial stress, transverse shear and normal stresses from  $x = 10\%L$  towards the left end can be observed. The first improvement comes from the iDQM

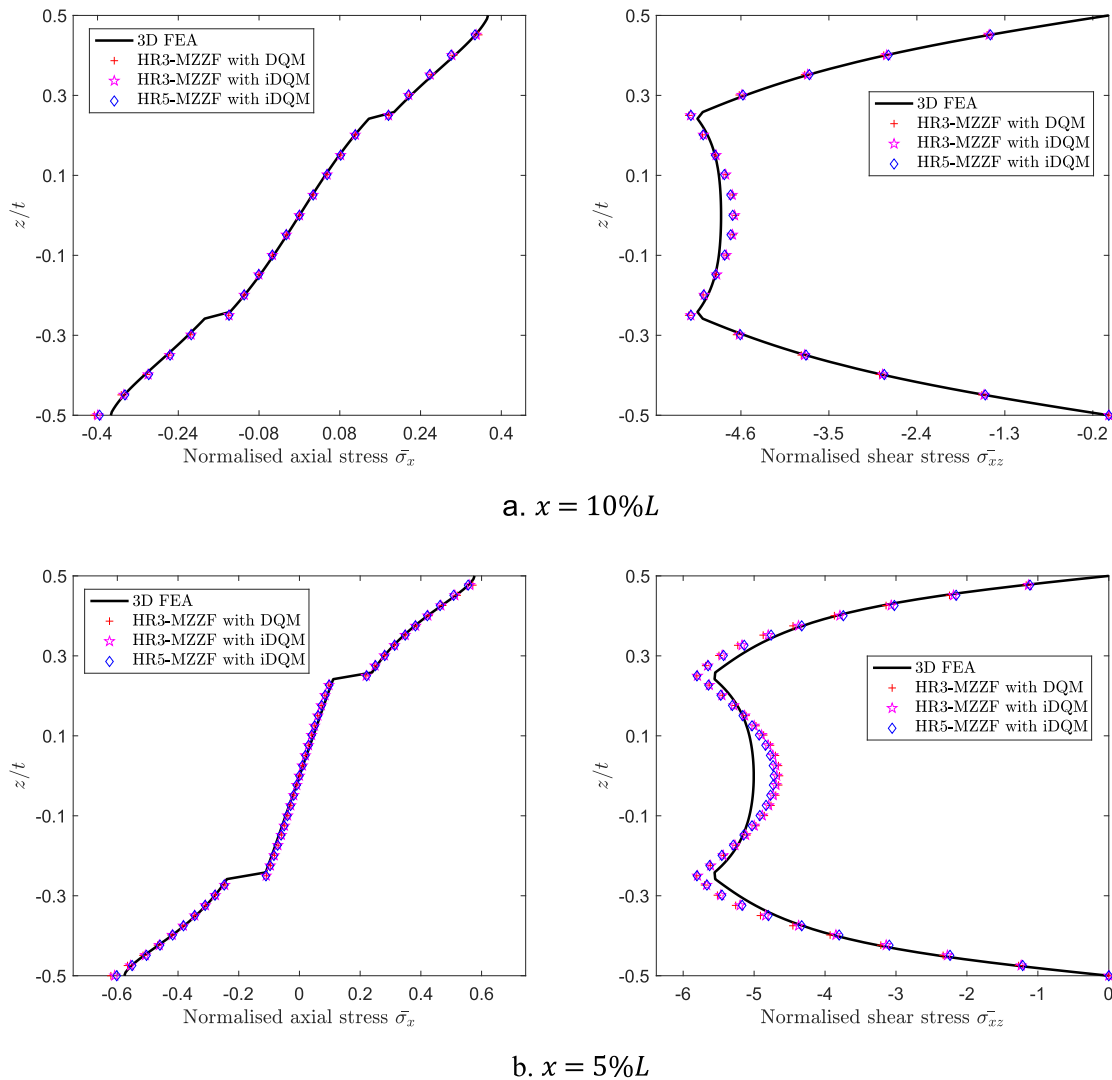


Fig. 15. Normalised axial and transverse shear stresses at the locations 10%, 5% of span from the left clamp (VAT A).

solution compared to the DQM solution. The second improvement is due to the richer kinematics of the fifth-order compared to the third-order assumption. Table 7.

Finally, validation of Cauchy’s equilibrium condition is conducted for point-wise positions following Eqs. 57 and 58, respectively. The residuals of the stress equilibrium are plotted in Fig. 17 for grid points in the middle of each ply and in Fig. 18 for an average ESL comparison. Although local errors are observed for both DQM and iDQM solutions, these errors are at least one

order of magnitude lower than those from the Abaqus solution presented in Fig. 19. Note, the *gradient* function in MATLAB is used for differentiating stresses in both the *x*- and *z*-axis for the Abaqus data. These data are exported from nodal stresses of 800 grid points along the beam axis and 121 grid points through the beam thickness. In addition, the interlaminar jumps do not affect this comparison as the equilibrium is assessed at the middle of each ply. Comparing the point-wise residuals of strong-form solutions (Fig. 17), the residuals by iDQM are slightly smaller than those

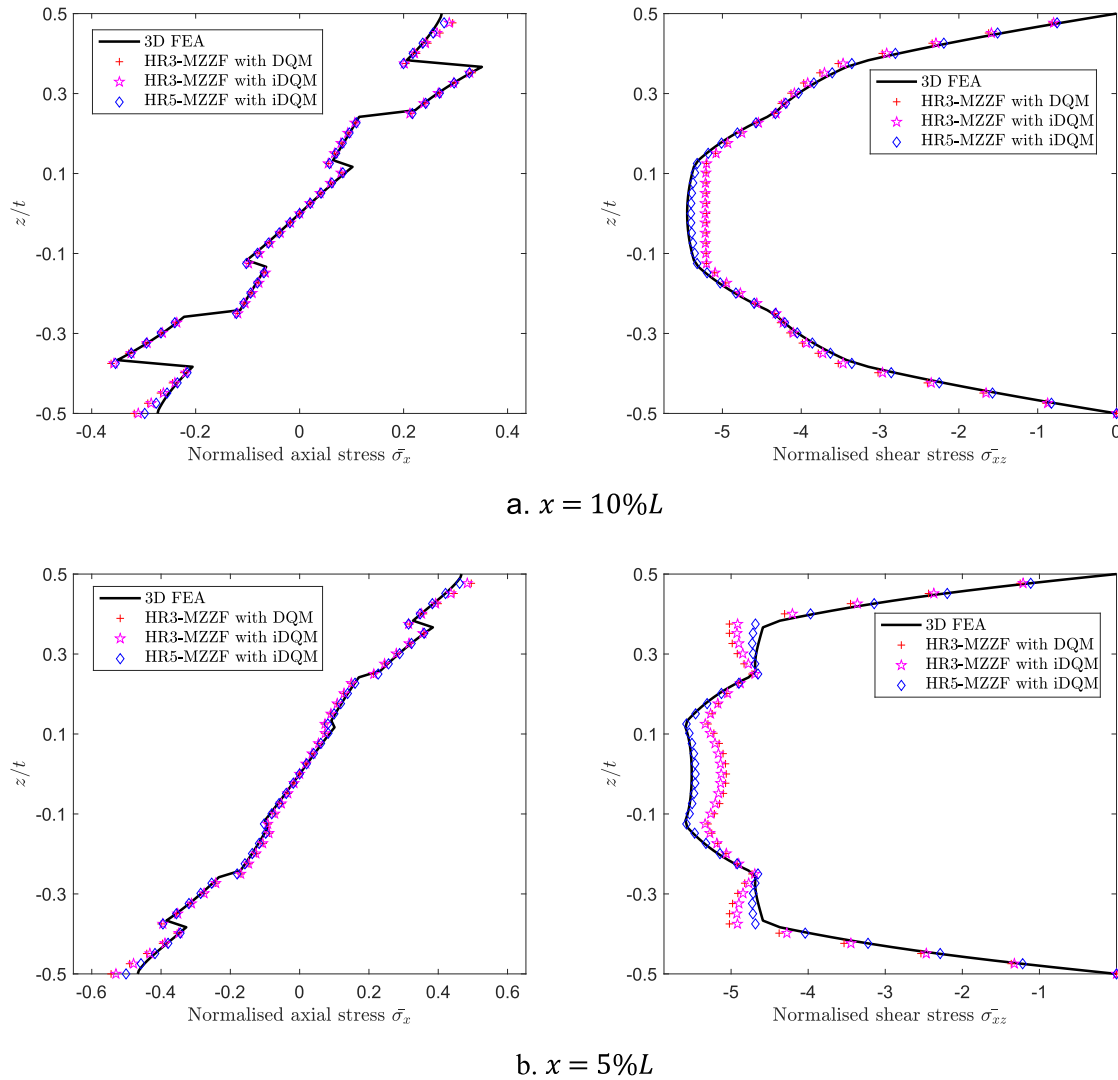
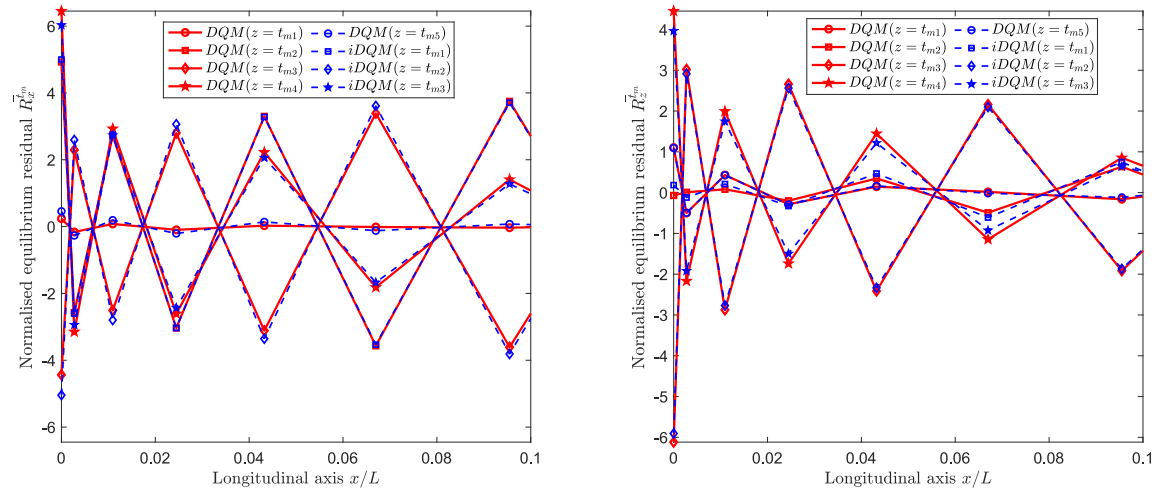


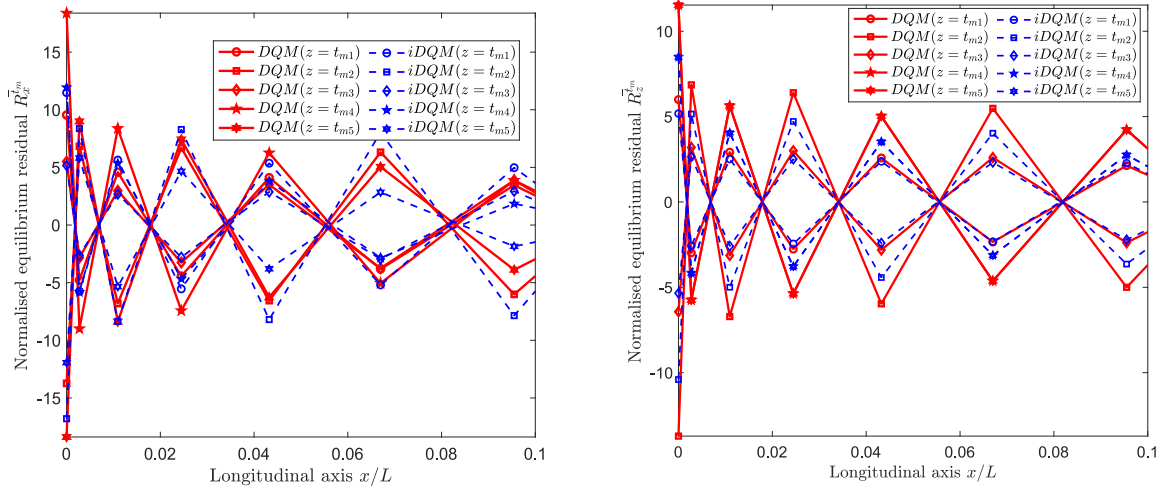
Fig. 16. Normalised axial and transverse shear stresses at the locations 10%, 5% of span from the left clamp (VAT B).

Table 7  
Normalised maximum deflection, axial stress and shear stress for clamped VAT beams.

Laminate	Model	0.1L			0.5L		
		$\bar{\sigma}_x^{min}$	$\bar{\sigma}_x^{max}$	$\bar{\tau}_{xz}^{max}$	$\bar{\sigma}_x^{min}$	$\bar{\sigma}_x^{max}$	$\bar{w}$
VAT A	3D Abaqus	-0.3735	0.3735	5.1437	-0.1709	0.1709	8.1686 E-07
	HR3-RZT with DQM	-0.3962	0.3963	5.2659	-0.1735	0.1735	8.3470E-07
	HR3-RZT with iDQM	-0.3897	0.3897	5.2425	-0.1735	0.1735	8.3472 E-07
	HR5-RZT with iDQM	-0.3971	0.3971	5.2392	-0.1715	0.1715	8.2433 E-07
VAT B	3D Abaqus	-0.3506	0.3506	5.4467	-0.2375	0.2375	8.3796 E-07
	HR3-RZT with DQM	-0.3627	0.3627	5.2064	-0.2262	0.2262	8.0078 E-07
	HR3-RZT with iDQM	-0.3571	0.3571	5.2194	-0.2262	0.2262	8.0076 E-07
	HR5-RZT with iDQM	-0.3542	0.3542	5.4000	-0.2387	0.2388	8.4713 E-07

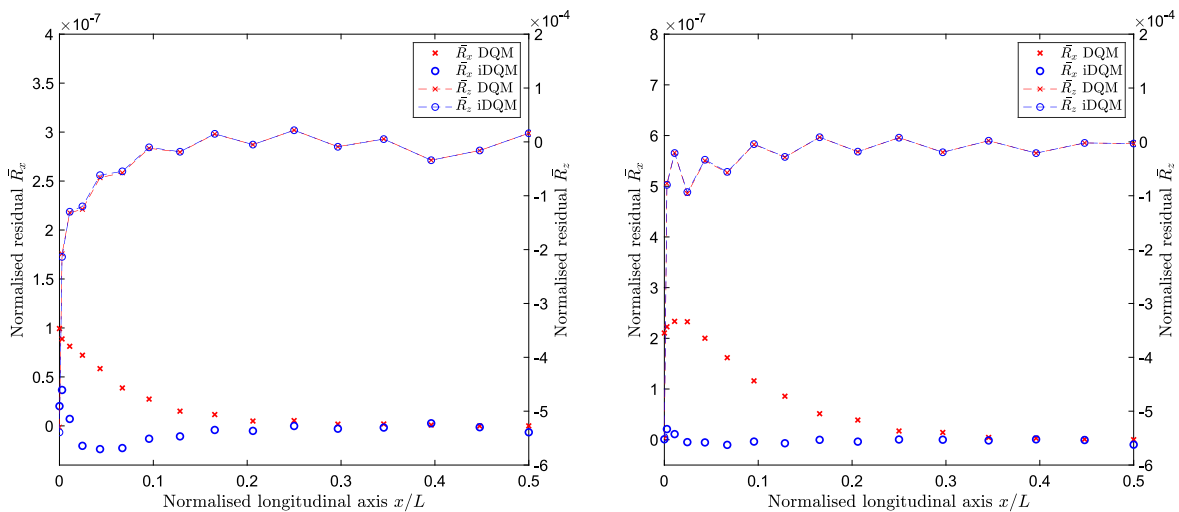


a. VAT A



b. VAT B

Fig. 17. Normalised Cauchy's equilibrium residual along the beam axis for points in the middle of each ply.



a. VAT A

b. VAT B

Fig. 18. Normalised Cauchy's equilibrium residual along the beam axis by integrating the residuals at every point through thickness (ESL concept).

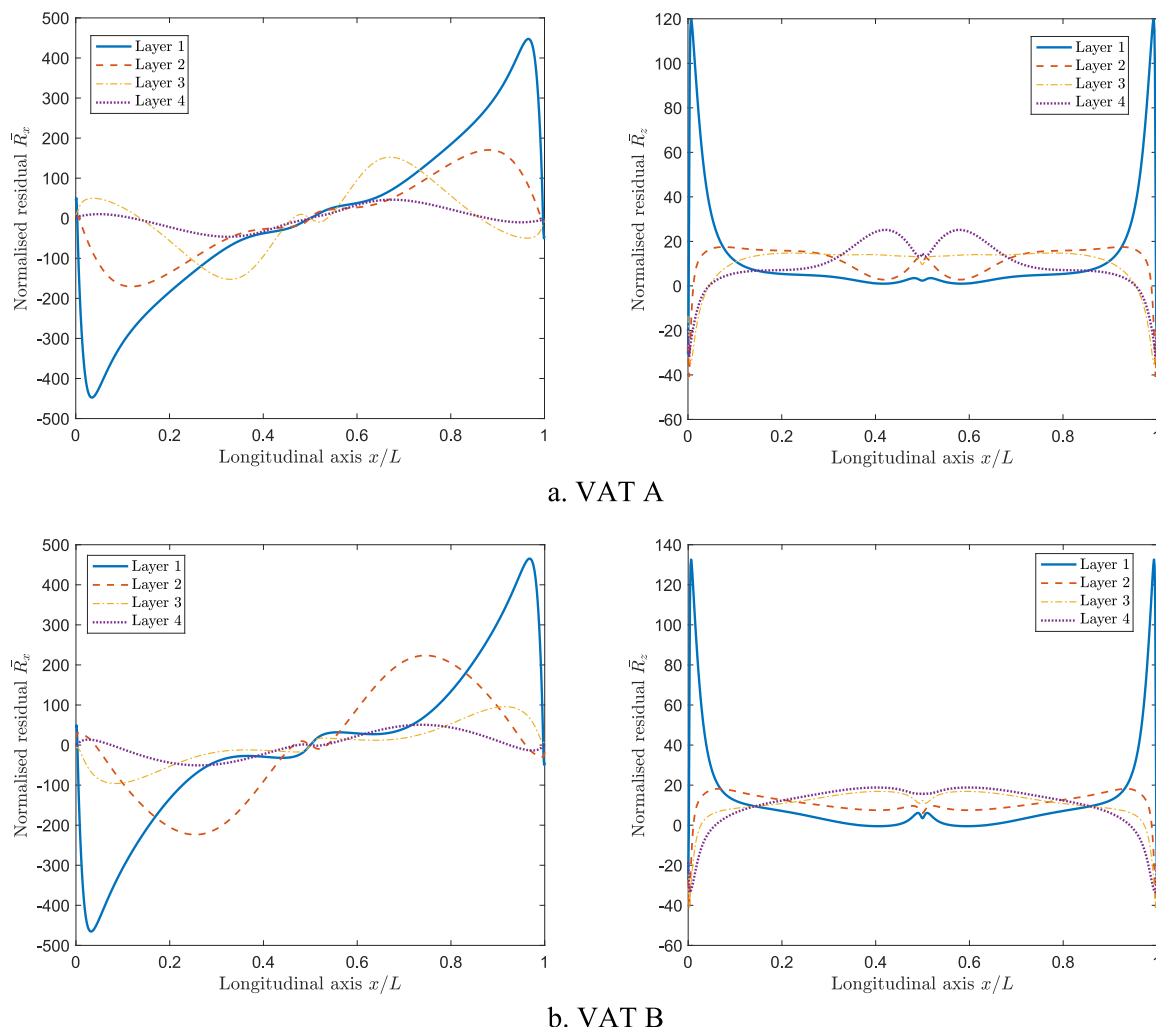


Fig. 19. Normalised Cauchy's equilibrium residual along the beam axis for points in the middle of each ply (Abaqus 3D solution).

from the DQM solution, especially near the clamped boundary. While the residual  $\bar{R}_z$  is almost the same comparing the iDQM and DQM solutions, the residual  $\bar{R}_x$  from the iDQM solution is much smaller compared to that from the DQM solution for points less than 30% of span from the clamped boundaries. This comparison together with stress plots confirm the efficiency of iDQM compared to DQM in analysing constant- and variable-stiffness laminated beams using the same Hellinger-Reissner mixed formulation.

#### 4. Conclusions

A framework for mixed inverse differential quadrature methods (mixed-iDQM) is proposed for flexural analysis of laminated beams. Based on a third-order zigzag displacement field and a Hellinger-Reissner (HR) mixed strain energy formulation developed previously, the governing equations and boundary conditions are rewritten in a new form which takes the first derivatives of stress resultants and displacements as primary functional unknowns. Fifth-order linear zigzag kinematics are also added to investigate the effect of a higher-order displacement assumption on different layup configurations. Numerical implementation is conducted for various constant-stiffness laminated beams under simply-supported, clamped and cantilevered conditions. It is shown that the mixed-iDQM always performs as well as or better than DQM for all cases analysed. In addition, a significant improve-

ment in accuracy of the transverse shear and normal stresses near the clamped end where the stress resultants vary rapidly is observed. A possible explanation for this improvement is that shear and transverse normal stresses are computed from the first and second derivatives of stress resultants, *i.e.* axial force, moment and higher-order moments. Using Lagrange polynomials to approximate the first derivatives results in fewer differentiation operations, thereby diminishing the computational error arising from solution of the system equations and computation of stresses. Further verification is performed for variable angle tow laminated beams and Cauchy's equilibrium condition is checked from the stress outputs of the model. Numerical results show that residuals of the stress equilibrium obtained from mixed-iDQM are smaller than those from DQM, thereby indicating the efficiency of iDQM in solving multi-functional mechanics problems. Finally, we show that the third-order linear zigzag displacement field is sufficient for stress analysis of most moderately thick laminated beams considered, but a fifth-order linear zigzag may be needed in complex variable angle layup configurations.

#### Declaration of Competing Interest

The authors declare that they have no known competing financial interests or personal relationships that could have appeared to influence the work reported in this paper.

## Acknowledgments

L.C. Trinh, S.O. Ojo and P.M. Weaver would like to acknowledge funding from the Science Foundation Ireland (SFI) for the award of a Research Professor grant (Varicomp: 15/RP/2773). R.M.J. Groh would like to acknowledge the Royal Academy of Engineering under the Research Fellowship scheme [Grant No. RF\201718\17178].

## References

- Ambartsumian, S.A., 1958. On a general theory of anisotropic shells. *J. Appl. Math. Mech.* 22, 305–319.
- Auricchio, F., Balduzzi, G., Khoshgoftar, M.J., Rahimi, G., Sacco, E., 2014. Enhanced modeling approach for multilayer anisotropic plates based on dimension reduction method and Hellinger-Reissner principle. *Compos. Struct.* 118, 622–633.
- Auricchio, F., Balduzzi, G., Lovadina, C., 2010. A new modeling approach for planar beams: finite-element solutions based on mixed variational derivations. *J. Mech. Mater. Struct.* 5, 771–794.
- Auricchio, F., Balduzzi, G., Lovadina, C., 2015. The dimensional reduction approach for 2D non-prismatic beam modelling: a solution based on Hellinger-Reissner principle. *Int. J. Solids Struct.* 63, 264–276.
- Baccocchi, M., Eisenberger, M., Fantuzzi, N., Tornabene, F., Viola, E., 2016. Vibration analysis of variable thickness plates and shells by the Generalized Differential Quadrature method. *Compos. Struct.* 156, 218–237.
- Barut, A., Madenci, E., Tessler, A., 2012. A Refined Zigzag Theory for Laminated Composite and Sandwich Plates Incorporating Thickness Stretch Deformation. Barut, A., Madenci, E., Tessler, A., 2013. C0-continuous triangular plate element for laminated composite and sandwich plates using the 2,2 – Refined Zigzag Theory. *Compos. Struct.* 106, 835–853.
- Batra, R.C., Vidoli, S., 2002. Higher-order piezoelectric plate theory derived from a three-dimensional variational principle. *AIAA J.* 40, 91–104.
- Bellman, R., Kashef, B.G., Casti, J., 1972. Differential quadrature: a technique for the rapid solution of nonlinear partial differential equations. *J. Comput. Phys.* 10, 40–52.
- Bert, C.W., Malik, M., 1996. Differential quadrature method in computational mechanics: a review. *Appl. Mech. Rev.* 49, 1–28.
- Cottrell, J.A., Hughes, T.J.R., Bazilevs, Y., 2009. *Isogeometric Analysis: Toward Integration of CAD and FEA*. John Wiley & Sons.
- Di Sciuva, M., 1984. A refinement of the transverse shear deformation theory for multilayered orthotropic plates. *L'aerotecnica missile e spazio* 62, 84–92.
- Di Sciuva, M., Sorrenti, M., 2019. Bending and free vibration analysis of functionally graded sandwich plates: an assessment of the Refined Zigzag Theory. *J. Sandwich Struct. Mater.*
- Eftekhari, S.A., Farid, M., Khani, M., 2009. Dynamic analysis of laminated composite coated beams carrying multiple accelerating oscillators using a coupled finite element-differential quadrature method. *J. Appl. Mech.* 76.
- Eftekhari, S.A., Jafari, A.A., 2012. Mixed finite element and differential quadrature method for free and forced vibration and buckling analysis of rectangular plates. *Appl. Math. Mech.* 33, 81–98.
- Faghih Shojaei, M., Yavari, A., 2019. Compatible-strain mixed finite element methods for 3D compressible and incompressible nonlinear elasticity. *Comput. Methods Appl. Mech. Eng.*, 357
- Fantuzzi, N., Baccocchi, M., Tornabene, F., Viola, E., Ferreira, A.J.M., 2015. Radial basis functions based on differential quadrature method for the free vibration analysis of laminated composite arbitrarily shaped plates. *Compos. B Eng.* 78, 65–78.
- Fantuzzi, N., Tornabene, F., Viola, E., 2014. Generalized Differential Quadrature Finite Element Method for vibration analysis of arbitrarily shaped membranes. *Int. J. Mech. Sci.* 79, 216–251.
- Fares, M.E., Elmarghany, M.K., 2008. A refined zigzag nonlinear first-order shear deformation theory of composite laminated plates. *Compos. Struct.* 82, 71–83.
- Ferreira, A.J.M., Carrera, E., Cinefra, M., Viola, E., Tornabene, F., Fantuzzi, N., Zenkour, A.M., 2014. Analysis of thick isotropic and cross-ply laminated plates by generalized differential quadrature method and a Unified Formulation. *Compos. B Eng.* 58, 544–552.
- Ferreira, A.J.M., Roque, C.M.C., Carrera, E., Cinefra, M., 2011. Analysis of thick isotropic and cross-ply laminated plates by radial basis functions and a Unified Formulation. *J. Sound Vib.* 330, 771–787.
- Flores, F.G., Oller, S., Nallim, L.G., 2018. On the analysis of non-homogeneous laminates using the refined zigzag theory. *Compos. Struct.* 204, 791–802.
- Gherlone, M., 2013. On the use of zigzag functions in equivalent single layer theories for laminated composite and sandwich beams: a comparative study and some observations on external weak layers. *J. Appl. Mech.* 80, 1–19.
- Groh, R.M.J., 2015. Non-classical Effects in Straight-Fibre and Towsteered Composite Beams and Plates Doctoral thesis. Department of Aerospace Engineering, University of Bristol.
- Groh, R.M.J., Tessler, A., 2017. Computationally efficient beam elements for accurate stresses in sandwich laminates and laminated composites with delaminations. *Comput. Methods Appl. Mech. Eng.* 320, 369–395.
- Groh, R.M.J., Weaver, P.M., 2015. On displacement-based and mixed-variational equivalent single layer theories for modelling highly heterogeneous laminated beams. *Int. J. Solids Struct.* 59, 147–170.
- Groh, R.M.J., Weaver, P.M., 2016. A computationally efficient 2D model for inherently equilibrated 3D stress predictions in heterogeneous laminated plates. Part I: model formulation. *Compos. Struct.* 156, 171–185.
- Groh, R.M.J., Weaver, P.M., 2016. A computationally efficient 2D model for inherently equilibrated 3D stress predictions in heterogeneous laminated plates. Part II: model validation. *Compos. Struct.* 156, 186–217.
- Groh, R.M.J., Weaver, P.M., Tessler, A., 2015. Application of the Refined Zigzag Theory to the Modeling of Delaminations in Laminated Composites. NASA/TM-2015-218808.
- Gürdal, Z., Olmedo, R., 1993. In-plane response of laminates with spatially varying fiber orientations - variable stiffness concept. *AIAA J.* 31, 751–758.
- Hegen, D., 1996. Element-free Galerkin methods in combination with finite element approaches. *Comput. Methods Appl. Mech. Eng.* 135, 143–166.
- Hughes, J.R.T., 1987. *The Finite Element Method: Linear Static and Dynamic Finite Element Analysis*. Dover Publication, INC., Mineola, New York.
- Iurlaro, L., Gherlone, M., Di Sciuva, M., 2015. The (3,2)-Mixed Refined Zigzag Theory for generally laminated beams: Theoretical development and C0 finite element formulation. *Int. J. Solids Struct.* 73–74, 1–19.
- Iurlaro, L., Gherlone, M., Di Sciuva, M., Tessler, A., 2015. Refined Zigzag Theory for laminated composite and sandwich plates derived from Reissner's Mixed Variational Theorem. *Compos. Struct.* 133, 809–817.
- Jones, R., 1998. *Mechanics of Composite Materials*. Taylor & Francis Ltd., London, UK.
- Lekhnitskii, S.G., 1935. Strength calculation of composite beams. *Vestnik inzhn i tekhnikov* 9.
- Liew, K.M., Huang, Y.Q., Reddy, J.N., 2003. Vibration analysis of symmetrically laminated plates based on FSDT using the moving least squares differential quadrature method. *Comput. Methods Appl. Mech. Eng.* 192, 2203–2222.
- Liu, B., Zhao, L., Ferreira, A.J.M., Xing, Y.F., Neves, A.M.A., Wang, J., 2017. Analysis of viscoelastic sandwich laminates using a unified formulation and a differential quadrature hierarchical finite element method. *Compos. B Eng.* 110, 185–192.
- Lu, Y.Y., Belytschko, T., Gu, L., 1994. A new implementation of the element free Galerkin method. *Comput. Methods Appl. Mech. Eng.* 113, 397–414.
- Madeo, A., Casciaro, R., Zagari, G., Zinno, R., Zucco, G., 2014. A mixed isostatic 16 dof quadrilateral membrane element with drilling rotations, based on Airy stresses. *Finite Elem. Anal. Des.* 89, 52–66.
- Mai-Duy, N., Tran-Cong, T., 2001. Numerical solution of differential equations using multiquadric radial basis function networks. *Neural Networks* 14, 185–199.
- Mai-Duy, N., Tran-Cong, T., 2003. Approximation of function and its derivatives using radial basis function networks. *Appl. Math. Model.* 27, 197–220.
- Mantari, J.L., Canales, F.G., 2016. Finite element formulation of laminated beams with capability to model the thickness expansion. *Compos. B Eng.* 101, 107–115.
- Mantari, J.L., Oktem, A.S., Guedes Soares, C., 2012. A new higher order shear deformation theory for sandwich and composite laminated plates. *Compos. B Eng.* 43, 1489–1499.
- Mittal, R.C., Rohla, R., 2016. Numerical simulation of reaction-diffusion systems by modified cubic B-spline differential quadrature method. *Chaos, Solitons Fractals* 92, 9–19.
- Murakami, H., 1986. Laminated composite plate theory with improved in-plane responses. *J. Appl. Mech.* 53, 661–666.
- Nallim, L.G., Oller, S., Oñate, E., Flores, F.G., 2017. A hierarchical finite element for composite laminated beams using a refined zigzag theory. *Compos. Struct.* 163, 168–184.
- Ngo-Cong, D., Mai-Duy, N., Karunasena, W., Tran-Cong, T., 2010. Integrated-RBF network method for free vibration analysis of laminated composite plates. In: *IOP Conference Series: Materials Science and Engineering*, p. 10.
- Ngo-Cong, D., Mai-Duy, N., Karunasena, W., Tran-Cong, T., 2011. Free vibration analysis of laminated composite plates based on FSDT using one-dimensional IRBFN method. *Comput. Struct.* 89, 1–13.
- Nguyen, C.U., Ibrahimbegovic, A., 2020. Visco-plasticity stress-based solid dynamics formulation and time-stepping algorithms for stiff case. *Int. J. Solids Struct.* 196–197, 154–170.
- Ojo, S.O., Patni, M., Weaver, P.M., 2019. Comparison of strong and weak formulations for 3D stress analysis of composite beams. *Int. J. Solids Struct.* 178–179, 145–166.
- Ojo, S.O., Trinh, L.C., Khalid, H.M., Weaver, P.M., 2020. Inverse differential quadrature method: mathematical formulation and error analysis, Submitted to *Proceedings of the royal society A*.
- Özütök, A., Madenci, E., 2017. Static analysis of laminated composite beams based on higher-order shear deformation theory by using mixed-type finite element method. *Int. J. Mech. Sci.* 130, 234–243.
- Pagano, N.J., 1969. Exact solutions for composite laminates in cylindrical bending. *J. Compos. Mater.* 3, 398–411.
- Patni, M., Minera, S., Groh, R.M.J., Pirrera, A., Weaver, P.M., 2018. Three-dimensional stress analysis for laminated composite and sandwich structures. *Compos. B Eng.* 155, 299–328.
- Patni, M., Minera, S., Groh, R.M.J., Pirrera, A., Weaver, P.M., 2019. On the accuracy of localised 3D stress fields in tow-steered laminated composite structures. *Compos. Struct.* 225.

- Quan, J.R., Chang, C.T., 1989. New insights in solving distributed system equations by the quadrature method - I. Analysis 1989. *Computers & Chemical Engineering* 13, 779–788.
- Reddy, J.N., 2006. *An Introduction to the Finite Element Method (Third Edition)*, Third Edition ed. McGrawHill.
- Shu, C., 2000. *Differential Quadrature and its Application in Engineering*. Springer, London.
- Shu, C., Richards, B.E., 1992. Parallel simulation of incompressible viscous flows by generalized differential quadrature. *Comput. Syst. Eng.* 3, 271–281.
- Smith, G.D., 1985. *Numerical Solution of Partial Differential Equations: Finite Difference Methods*. Oxford University Press.
- Taylor, R.L., Zienkiewicz, O.C., Oñate, E., 1998. A hierarchical finite element method based on the partition of unity. *Comput. Methods Appl. Mech. Eng.* 152, 73–84.
- Tessler, A., 2015. Refined zigzag theory for homogeneous, laminated composite, and sandwich beams derived from Reissner's mixed variational principle. *Meccanica* 50, 2621–2648.
- Tessler, A., Di Sciuva, M., Gherlone, M., 2007. Refinement of Timoshenko beam theory for composite and sandwich beams using zigzag kinematics, NASA/TP-2007-215086.
- Tessler, A., Di Sciuva, M., Gherlone, M., 2009. Refined Zigzag Theory for Laminated Composite and Sandwich Plates, NASA/TP-2009-215561.
- Thurnherr, C., Groh, R.M.J., Ermanni, P., Weaver, P.M., 2016. Higher-order beam model for stress predictions in curved beams made from anisotropic materials. *Int. J. Solids Struct.* 97–98, 16–28.
- Timoshenko, S., Goodier, J., 1970. *Theory of Elasticity*. McGraw-Hill, New York.
- Tornabene, F., Fantuzzi, N., Viola, E., Carrera, E., 2014. Static analysis of doubly-curved anisotropic shells and panels using CUF approach, differential geometry and differential quadrature method. *Compos. Struct.* 107, 675–697.
- Trinh, L.C., Groh, R.M.J., Zucco, G., Weaver, P.M., 2020. A strain-displacement mixed formulation based on the modified couple stress theory for the flexural behaviour of laminated beams. *Compos. B Eng.* 185, 107740.
- Versino, D., Gherlone, M., Di Sciuva, M., 2014. Four-node shell element for doubly curved multilayered composites based on the Refined Zigzag Theory. *Compos. Struct.* 118, 392–402.
- Viebahn, N., Steeger, K., Schröder, J., 2018. A simple and efficient Hellinger-Reissner type mixed finite element for nearly incompressible elasticity. *Comput. Methods Appl. Mech. Eng.* 340, 278–295.
- Vo, T.P., Nguyen, T.-K., Thai, H.-T., Lanc, D., Karamanli, A., 2017. Flexural analysis of laminated composite and sandwich beams using a four-unknown shear and normal deformation theory. *Compos. Struct.* 176, 388–397.
- Vo, T.P., Thai, H.-T., 2012. Static behavior of composite beams using various refined shear deformation theories. *Compos. Struct.* 94, 2513–2522.
- Wu, X., Ren, Y., 2007. Differential quadrature method based on the highest derivative and its applications. *J. Comput. Appl. Math.* 205, 239–250.
- Wu, Y., Xing, Y., Liu, B., 2018. Analysis of isotropic and composite laminated plates and shells using a differential quadrature hierarchical finite element method. *Compos. Struct.* 205, 11–25.
- Zenkour, A.M., 1999. Transverse shear and normal deformation theory for bending analysis of laminated and sandwich elastic beams. *Mech. Compos. Mater. Struct.* 6, 267–283.
- Zong, Z., Zhang, Y., 2009. *Advanced Differential Quadrature Methods*. Taylor and Francis Group.
- Zucco, G., Groh, R.M.J., Madeo, A., Weaver, P.M., 2016. Mixed shell element for static and buckling analysis of variable angle tow composite plates. *Compos. Struct.* 152, 324–338.